

PAPER • OPEN ACCESS

Unconventional superconductivity in $\text{Cu}_x\text{Bi}_2\text{Se}_3$ from magnetic susceptibility and electrical transport

To cite this article: Yifei Fang *et al* 2020 *New J. Phys.* **22** 053026

View the [article online](#) for updates and enhancements.

Recent citations

- [Phonon softening and higher-order anharmonic effect in the superconducting topological insulator \$\text{Sr}_x\text{Bi}_2\text{Se}_3\$](#)
Mingtao Li *et al*



PAPER

Unconventional superconductivity in $\text{Cu}_x\text{Bi}_2\text{Se}_3$ from magnetic susceptibility and electrical transport

OPEN ACCESS

RECEIVED

20 November 2019

REVISED

10 February 2020

ACCEPTED FOR PUBLICATION

13 March 2020

PUBLISHED

7 May 2020

Original content from this work may be used under the terms of the [Creative Commons Attribution 4.0 licence](https://creativecommons.org/licenses/by/4.0/).

Any further distribution of this work must maintain attribution to the author(s) and the title of the work, journal citation and DOI.

Yifei Fang^{1,2} , Wen-Long You^{3,4} and Mingtao Li^{5,6} ¹ Key Laboratory of High Power Laser Materials, Shanghai Institute of Optics and Fine Mechanics, Chinese Academy of Sciences, Shanghai, 201800, People's Republic of China² Department of Physics, Fudan University, Shanghai 200433, People's Republic of China³ College of Science, Nanjing University of Aeronautics and Astronautics, Nanjing, 211106, People's Republic of China⁴ School of Physical Science and Technology, Soochow University, Suzhou, Jiangsu 215006, People's Republic of China⁵ Center for High Pressure Science and Technology Advanced Research, Shanghai 201203, People's Republic of China⁶ Author to whom any correspondence should be addressed.E-mail: mingtaoli04@gmail.com**Keywords:** topological material, critical parameters, unconventional superconductivitySupplementary material for this article is available [online](#)**Abstract**

Although the Cu doped Bi_2Se_3 topological insulator was discovered and intensively studied for almost a decade, its electrical and magnetic properties in normal state, and the mechanism of 'high- T_c ' superconductivity regarding the relatively low-carrier density are still not addressed yet. In this work, we report a systematic investigation of magnetic susceptibility, critical fields, and electrical transport on the nominal $\text{Cu}_{0.20}\text{Bi}_2\text{Se}_3$ single crystals with $T_c^{\text{onset}} = 4.18$ K, the highest so far. The composition analysis yields the Cu stoichiometry of $x = 0.09(1)$. The magnetic susceptibility shows considerable anisotropy and an obvious kink at around 96 K was observed in the magnetic susceptibility for $H \parallel c$, which indicates a charge density anomaly. The electrical transport measurements indicate the two-dimensional (2D) Fermi liquid behavior at low temperatures with a high Kadowaki–Woods ratio, $A/\gamma^2 = 30.3a_0$. The lower critical field at 0 K limit was extracted to be 6.0 Oe for $H \parallel ab$. In the clean limit, the ratio of energy gap to T_c was determined to be $\Delta_0/k_B T_c = 2.029 \pm 0.124$ exceeding the standard BCS value 1.764, suggesting $\text{Cu}_{0.09}\text{Bi}_2\text{Se}_3$ is a strong-coupling superconductor. The in-plane penetration depth at 0 K was calculated to be 1541.57 nm, resulting in an unprecedented high ratio of $T_c/\lambda^{-2}(0) \cong 9.86$. Moreover, the ratio of T_c to Fermi temperature is estimated to be $T_c/T_F^{2D} = 0.034$. Both ratios fall into the region of unconventional superconductivity according to Uemura's regime, supporting the unconventional superconducting mechanism in $\text{Cu}_x\text{Bi}_2\text{Se}_3$. Finally, the enhanced T_c value higher than 4 K is proposed to arise from the increased density of states at Fermi energy and strong electron–phonon interaction induced by the charge density instability.

1. Introduction

The superconducting critical temperature (T_c) up to 3.8 K in doped superconducting topological insulators such as $\text{Cu}_x\text{Bi}_2\text{Se}_3$ are unexpectedly 'high' for a low carrier density semiconductor [1]. According to the quantum oscillations results [2], the Fermi wave number k_F in $\text{Cu}_x\text{Bi}_2\text{Se}_3$ is increased from 0.69 nm^{-1} to 0.97 nm^{-1} by Cu doping. Such value lies within the range of $0.1\text{--}1 \text{ nm}^{-1}$ for typical densities in a classical two-band single valley semiconductor [3], in which the density of states (DOS) is only about one-tenth of that of a metal. Actually, the superconductivity was also observed in some semiconductors with T_c far below 1 K, such as SrTiO_3 ($T_c \sim 0.05\text{--}0.29$ K, $n_e = 0.65$ to $42.4 \times 10^{20} \text{ cm}^{-3}$) [3, 4], GeTe ($T_c \sim 0.07\text{--}0.3$ K, $n_e = 8.6$ to $15.2 \times 10^{20} \text{ cm}^{-3}$) [5], and SnTe ($T_c \sim 0.034\text{--}0.214$ K, $n_p = 7.5$ to $20.0 \times 10^{20} \text{ cm}^{-3}$) [6]. To compare with these systems, the T_c value of $\text{Cu}_x\text{Bi}_2\text{Se}_3$ is relatively 'high' given it is a highly doped narrow semiconductor with lower carrier density. However, the mechanism of such anomalous enhanced T_c phenomenon remains unclear despite nearly a decade of extensive research.

The emergence and enhancement of superconductivity may occur in various cases by tailoring the ground states of quantum materials. For example, suppression of charge density wave (CDW) by chemical doping or pressure is observed in many systems [7–10], including low dimensional layered Cu_xTiSe_2 and three dimensional (3D) alloys $\text{Lu}(\text{Pt}_{1-x}\text{Pd}_x)_2\text{In}$ and $(\text{Sr}, \text{Ca})_3\text{Ir}_4\text{Sn}_{13}$, 3D oxides $\text{Ba}_{1-x}\text{K}_x\text{BiO}_3$. Similarly, the magnetic ordering or spin density wave (SDW) have also been suppressed in strongly correlated heavy fermions materials, high- T_c cuprates and iron-based superconductors [11–13]. Lastly, the value of T_c can be significantly suppressed by introducing disorders [14], leading to metal–insulator transition. Note that such mechanism may be also relevant to superconducting semiconductors, since a large number of disorders are expected inside.

In this work, we revisit the superconducting $\text{Cu}_x\text{Bi}_2\text{Se}_3$ system, which is widely studied in the past but rarely emphasizing on the magnetic susceptibility and electrical transport properties in the normal state. Interestingly, we observed $T_c = 4.18$ K in $\text{Cu}_{0.09}\text{Bi}_2\text{Se}_3$ for our sample, the highest value to date. In addition, for the first time, we reveal a charge density anomaly at around 96 K in the $\text{Cu}_{0.09}\text{Bi}_2\text{Se}_3$ crystal from the magnetic susceptibility in the normal state, which is reminiscent of unconventional superconductivity proximity to CDW. We show the $\text{Cu}_{0.09}\text{Bi}_2\text{Se}_3$ displays the 2D Fermi liquid behavior at low temperature with a high Kadowaki–Woods ratio, $A/\gamma^2 = 30.3a_0$, as may be enhanced by proximity to charge density instability and/or strong electronic anisotropy. Furthermore, we obtain the upper and lower critical fields from the measurement of temperature dependent magnetic susceptibility under different fields. We find the $\text{Cu}_{0.09}\text{Bi}_2\text{Se}_3$ is a strong-coupling superconductor with $\Delta_0/k_B T_c = 2.029 \pm 0.124$ exceeding the standard BCS value 1.764. Finally, we discuss the possible underlying mechanisms for the enhanced T_c higher than 4 K and the unconventional superconducting features. Importantly, we demonstrate the $\text{Cu}_{0.09}\text{Bi}_2\text{Se}_3$ belongs to one of unconventional superconducting families according to Uemura’s plot, with unprecedented high ratios of $T_c/\lambda^2(0) \cong 9.86$ and $T_c/T_F^{2D} = 0.034$ among superconducting semiconductors.

2. Experimental details

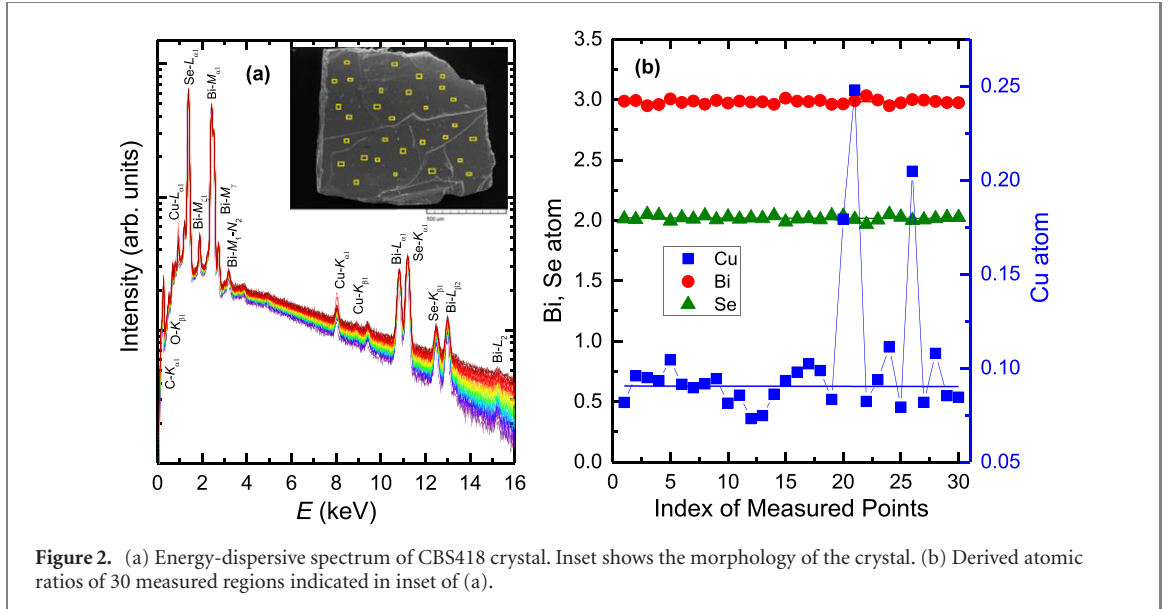
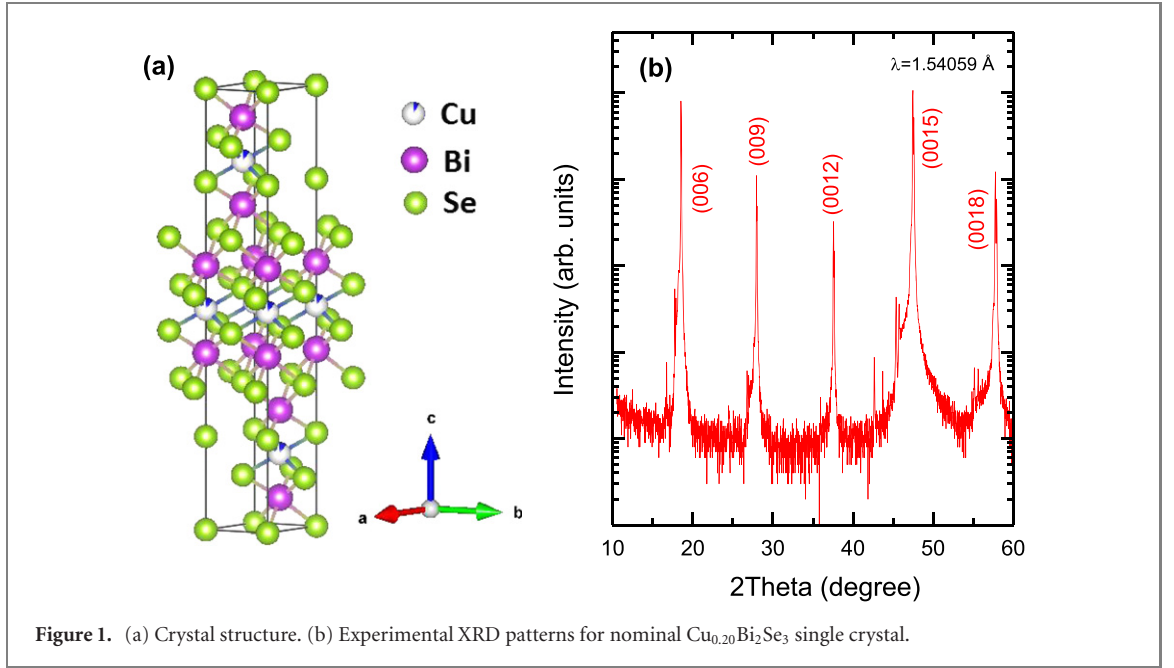
The samples were prepared using high purity (99.999%) elements in the nominal composition $\text{Cu}_x\text{Bi}_2\text{Se}_3$ ($x = 0.20$), as reported elsewhere [15, 16]. We find some crystals cleaved from the large batch are superconducting at 4.18 K (denoted as CBS418), which is higher than previous report [1]. The phase purity of obtained single crystals was examined by x-ray diffraction (XRD) measurements with $\text{Cu K}\alpha$ radiation. To check the homogeneity, we performed the measurements of the energy-dispersive spectrum on the sample with $T_c^{\text{onset}} = 4.18$ K. In addition, we also present the measurements of pure Bi_2Se_3 (denoted as BS) and nominal $\text{Cu}_{0.20}\text{Bi}_2\text{Se}_3$ with $T_c^{\text{onset}} = 3.79$ K (denoted as CBS379). The in-plane resistivity measurements were carried out on a physical property measurement system (PPMS-9, quantum design) using the standard four probes with silver paste as the contacts. The DC magnetic susceptibility and initial magnetizations curves were measured with a SQUID-VSM magnetometer (quantum design) at different magnetic fields and temperatures.

3. Results and discussion

3.1. Crystal structure and composition

Figures 1(a) and (b) show the crystal structure and XRD patterns as collected on $\text{Cu}_{0.20}\text{Bi}_2\text{Se}_3$ single crystal. The parent Bi_2Se_3 compound crystallizes to the rhombohedral structure with space group $R\bar{3}m$ (no. 166) [17]. As suggested by the previous report [1], the intercalated Cu atoms were in the van der Waals gap between Bi_2Se_3 layers, which partially occupy the octahedrally coordinated $3b$ (0, 0, 1/2) sites, as indicated in figure 1(a). Only a series of (00 l) reflections were observed and the background is clean, indicating the phase purity. This is consistent with those expected from the rhombohedral space group of Bi_2Se_3 [17].

To investigate the sample homogeneity, we performed composition analysis on the sample with the onset superconducting transition temperature $T_c^{\text{onset}} = 4.18$ K by energy dispersive x-ray spectroscopy (EDS). A total of 30 random EDS spectra locating at different regions were measured, as indicated by yellow frames in the inset of figure 2(a). The atomic ratios were plotted in figure 2(b). We observed that there are three measured regions with higher Cu content than others, where the Cu content is between 0.15 and 0.25. In these regions, all the element ratios of Bi and Se are very close to their stoichiometric composition, indicating the Bi and Se elements are generally homogeneous on a large scale. The remaining measured EDS spectrum yields an averaged composition $\text{Cu}_{0.09(1)}\text{Bi}_{2.02(2)}\text{Se}_{2.98(2)}$ (referred as $\text{Cu}_{0.09}\text{Bi}_2\text{Se}_3$), in which the Cu content ratio still fluctuates within 23% compared to the averaged value. This demonstrates the melt-grown crystal is quite inhomogeneous on a micrometer scale. It is reported that the distribution of Cu



content in the electrochemical synthesized samples shows a $\sim 19\%$ variation [18], which is slightly smaller than that in our melt-grown crystals. According to phase diagram reported by Kriener *et al* [18], the higher T_c phase is deemed to have a lower Cu doping level.

3.2. Magnetic susceptibility

Figure 3 shows the temperature dependence of volume susceptibility $\chi(T)$ measured under $H = 3$ Oe on one crystal with dimensions of $\sim 5.83 \times 4.67 \times 0.59$ mm³. We observe T_c^{onset} occurs at 4.18 K, which is the highest in doped Bi_2Se_3 to our knowledge. The apparent difference between zero-field cooling (ZFC) and field cooling (FC) is caused by the vortex pinning, which has been investigated in detail for $\text{Cu}_x\text{Bi}_2\text{Se}_3$ [15, 16]. Interestingly, the peak effect, a feature of anomalous vortex pinning phenomenon, is observed in the high quality clean $\text{Cu}_x\text{Bi}_2\text{Se}_3$ crystals [15, 16]. To estimate the volume shielding fraction, we take the demagnetization factor N into account, which can be calculated by [19]

$$N = \left[1 + \frac{3c}{4a} \left(1 + \frac{a}{b} \right) \right]^{-1}, \quad (1)$$

where a, b, c are dimensions ($2a \times 2b \times 2c$) of the experimental specimen with rectangular cuboid shape. According to equation (1), we obtain $N_{ab} = 0.107$ for $H \parallel ab$ and $N_c = 0.854$ for $H \parallel c$. The intrinsic

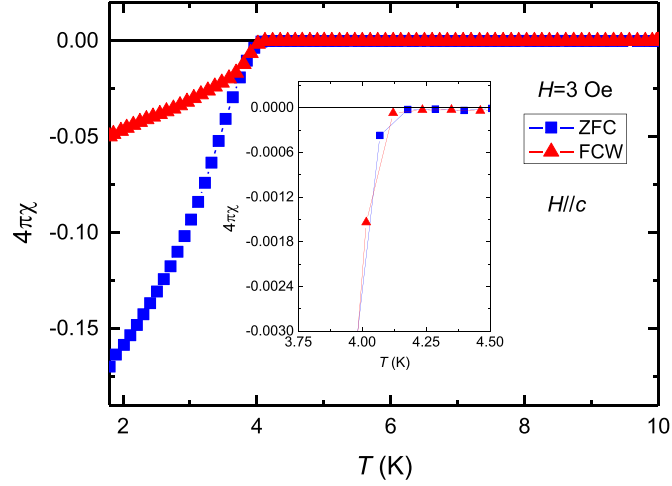


Figure 3. Volume susceptibility versus temperature $\chi(T)$ under 3 Oe for $H \parallel c$ in ZFC and FC modes. Inset shows the detailed region at the onset superconducting transition.

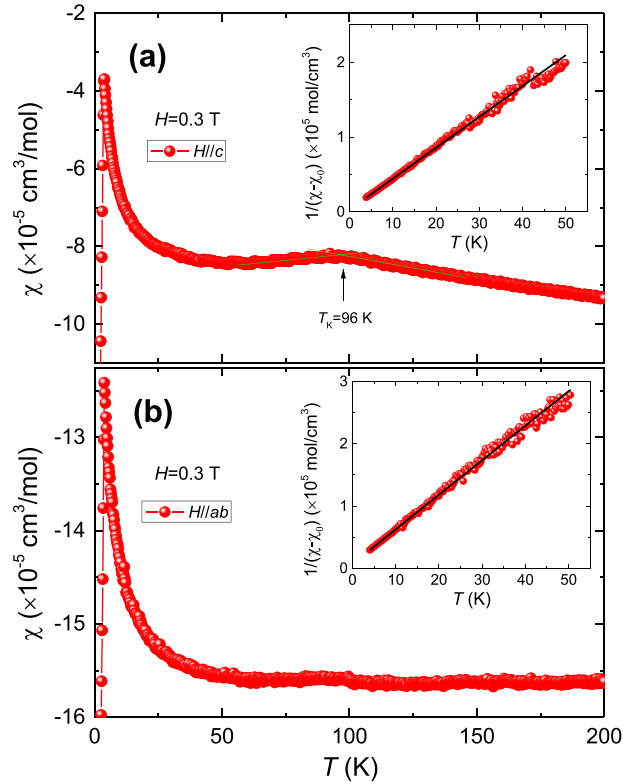


Figure 4. Temperature dependence of magnetic susceptibility under 0.3 T for (a) $H \parallel c$, (b) $H \parallel ab$. The insets is the Curie–Weiss fit.

volume susceptibility χ_{int} is given by

$$\chi_{\text{int}} = \chi_{\text{exp}} / (1 - N\chi_{\text{exp}}), \quad (2)$$

where χ_{exp} is the experimental measured susceptibility. As seen in figure 3, a 17% superconducting shielding fraction was estimated, which is consistent with other reports [1, 20–22].

To investigate the magnetic properties in normal state, we measured $\chi(T)$ under 0.3 T, as is plotted in figure 4. The magnetic susceptibility $\chi \equiv M/H$ for both $H \parallel c$ and $H \parallel ab$ shows a small negative background, essentially presenting a weak temperature dependence at high temperatures ($T > 96$ K). This indicates that the Larmor or Langevin diamagnetic and Landau diamagnetic contributions are larger than the sum of the spin Pauli paramagnetic susceptibility. With decreasing the temperature, the magnitude of χ firstly shows a quasilinear increase up to 96 K, below which a kink occurs. The drop of χ across the kink

temperature (T_k) implies a decrease of electronic DOS at Fermi energy (E_F). The quasilinear behavior of χ above the T_k and its weak temperature dependence have been widely observed in some CDW materials like Cu_xTiSe_2 [7], $\text{Lu}(\text{Pt}_{1-x}\text{Pd}_x)_2\text{In}$ [8], and $(\text{Sr}, \text{Ca})_3\text{Ir}_4\text{Sn}_{13}$ [9]. In $\text{Cu}_{0.09}\text{Bi}_2\text{Se}_3$, the superconductivity is induced only by Cu intercalation, which is in favor of Cu^{1+} non-magnetic state (as is in the case of interstitial site, see reference [23]). While the Cu has a possibility to substitute the Bi [23], which can create two holes and act as carrier acceptors to depress the carrier density. Therefore, almost all the ions in $\text{Cu}_x\text{Bi}_2\text{Se}_3$ are fully shelled, so a magnetic ordering seems to be highly impossible. The observed kink in $\chi(T)$ is likely to be attributed to the charge density anomaly, or possibly the CDW transition, below which the Fermi surface (FS) is partially or fully gapped resulting in the reduction of DOS at E_F . For this reason, the resistivity will sometimes display an upturn feature when the temperature crosses the T_k [7–9]. However, other factors, like changes in the effective carrier mass and the scattering rate [9], shall also be taken into account to interpret this upturn. Moreover, the weaker kink feature in $\chi^{ab}(T)$ implies that the measured sample has a prominent anisotropic bulk FS since it holds a layered crystal structure and the Bi–Se quintuple layers are weakly bonded by van der Waals force.

Using the electron diffraction measurements at room temperature, the existence of CDW was reported in other Cu intercalated Bi_2Se_3 -based topological insulators [24, 25]. However, the evidence of forming superlattice spots or diffusive order was given only in higher Cu doping content, e.g., >10 atom% for zero-valent intercalated $\text{Cu}_x\text{Bi}_2\text{Se}_3$ [24] and 5.6 atom% for Cu^{1+} intercalated $\text{Bi}_2\text{Te}_2\text{Se}$ [25]. Thus, the observed charge density anomaly in our crystal (~ 2 atom% for Cu^{1+} intercalation) is surprising, the content of which is close to the optimal level [1]. According to theoretical calculations [26, 27] and angle-resolved photoemission electron spectroscopy (ARPES) experiments [28, 29], the conduction bands are dominated by Bi- p_z orbitals and would be accumulated by the electron carriers through Cu doping, leading to the lift of Fermi level. Further, since the electron doping ($x \sim 0.12$) can induce large phonon singular electron–phonon interaction behavior and strong FS nesting in the Brillouin zone [27], it is likely that the charge density anomaly is related to the Bi_2Se_3 quintuple layers for nearly optimal electron-doped $\text{Cu}_x\text{Bi}_2\text{Se}_3$.

As seen in figure 4, the $\chi(T)$ shows an upward behavior below 50 K, which can be attributed to a tiny amount of paramagnetic defects in non-magnetic or weakly-correlated magnetic systems [8, 30]. Such upturn in $\chi(T)$ is also observed in other non-magnetic materials, for instance, $\text{Lu}(\text{Pt}_{1-x}\text{Pd}_x)_2\text{In}$ [8] and LaPtGe_3 ($T_c = 1.2$ K) superconductors [31]. Furthermore, we find the $\chi(T)$ curve between 5 K and 50 K could be well fitted by a modified Curie–Weiss law [32–34], reading

$$\chi = \chi_0 + \frac{C}{T - \Theta_{\text{cw}}}, \quad (3)$$

where C is Curie constant, Θ_{cw} is Weiss temperature, χ_0 is an isotropic temperature-independent term given by $\chi_0 = \chi_{\text{dia}} + \chi_{\text{para}} = \chi_{\text{core}} + \chi_{\text{Landau}} + \chi_{\text{vanVleck}} + \chi_{\text{Pauli}}$, in which χ_{core} is the diamagnetic (orbital) contribution from the atomic core electrons, χ_{Landau} is the diamagnetic (orbital) Landau susceptibility of the conduction electrons, χ_{vanVleck} is the paramagnetic (orbital) van Vleck susceptibility, and χ_{Pauli} is the paramagnetic (spin) Pauli susceptibility of conduction electrons. The fitted values for $H \parallel c$ and $H \parallel ab$ are $\chi_0^c(\chi_0^{ab}) = -89.3 \times 10^{-6}$ (-159×10^{-6}) $\text{cm}^3 \text{mol}^{-1}$, $C^c(C^{ab}) = -2.42 \times 10^{-4}$ (-1.80×10^{-4}) $\text{cm}^3 \text{K mol}^{-1}$, and $\Theta_{\text{cw}}^c(\Theta_{\text{cw}}^{ab}) = -1.25$ (-0.73) K. The Curie constant per mole of spins is given by [35]

$$C = \frac{N_A g^2 S(S+1) \mu_B^2}{3k_B} \equiv \frac{N_A \mu_{\text{eff}}^2 \mu_B^2}{3k_B}, \quad (4)$$

where N_A is Avogadro's number, g is the Landé g -factor, μ_B is the Bohr magneton, k_B is Boltzmann's constant, and $\mu_{\text{eff}} = g\sqrt{S(S+1)} = \sqrt{\frac{3k_B C}{N_A \mu_B^2}}$ is the effective moment of a spin in unit of μ_B (the orbital quantum number $L = 0$, $J = S$). Taking the Gaussian–CGS values of the fundamental constants, $N_A = 6.022 \times 10^{23} \text{ mol}^{-1}$, $k_B = 1.381 \times 10^{-16} \text{ erg K}^{-1}$, and $\mu_B = 9.274 \times 10^{-16} \text{ erg K}^{-1}$, μ_{eff} is given as $\mu_{\text{eff}} \approx \sqrt{7.99684C}$. The fitted Curie constants yield an effective moment of $\mu_{\text{eff}}^c = 0.044 \mu_B$ and $\mu_{\text{eff}}^{ab} = 0.038 \mu_B$ for $H \parallel c$ and $H \parallel ab$, respectively. On one hand, assuming the g -factor $g = 2.25$ typically found for Cu^{2+} cations [36], the net moment of Cu^{2+} ion is estimated to be $1.95 \mu_B$, which is much larger than experimental value of the effective moment. On the other hand, according to the Cu–Se binary diagram [37], the possible precipitated Cu_2Se phase is more favorable than the CuSe , so the paramagnetism arising from Cu^{2+} is also not promising from this point. For these reasons, we ascribe the observed anomaly at 96 K to charge density anomaly rather than the onset of magnetic ordering. The negative values of Θ^c and Θ^{ab} indicate there exists weak antiferromagnetic exchange interactions, likely originating from the defects since the Cu^{1+} is non-magnetic with $S = 0$.

Table 1. Magnetic parameters obtained by fitting and calculation for CBS418 crystal.

Properties	Units	Values
χ_0^c	$\text{cm}^3 \text{mol}^{-1}$	-89.3×10^{-6}
χ_0^{ab}	$\text{cm}^3 \text{mol}^{-1}$	-159×10^{-6}
C^c	$\text{cm}^3 \text{K mol}^{-1}$	-2.42×10^{-4}
C^{ab}	$\text{cm}^3 \text{K mol}^{-1}$	-1.80×10^{-4}
Θ_{cw}^c	K	-1.25
Θ_{cw}^{ab}	K	-0.73
μ_{eff}^c	μ_B	0.044
μ_{eff}^{ab}	μ_B	0.038
χ_{Pauli}	$\text{cm}^3 \text{mol}^{-1}$	47.4×10^{-6}
χ_{Landau}	$\text{cm}^3 \text{mol}^{-1}$	-419.8×10^{-6}
$\chi_{\text{core}}^{\text{ionic}}$	$\text{cm}^3 \text{mol}^{-1}$	-195.1×10^{-6}
$\chi_{\text{core}}^{\text{atomic}}$	$\text{cm}^3 \text{mol}^{-1}$	-215.1×10^{-6}
χ_0^{ionic}	$\text{cm}^3 \text{mol}^{-1}$	-56.8×10^{-5}
χ_0^{atomic}	$\text{cm}^3 \text{mol}^{-1}$	-58.8×10^{-5}
χ_P	$\text{cm}^3 \text{mol}^{-1}$	47.9×10^{-5}

Furthermore, one can estimate the χ_{Pauli} at $T = 0$ K using the relation [38]

$$\chi_{\text{Pauli}} = \frac{g^2}{4} \mu_B^2 N(E_F), \quad (5)$$

where $N(E_F)$ is the DOS at the E_F . Inserting $g = 2$ into equation (5) gives $\chi_{\text{Pauli}} = (3.233 \times 10^{-5})N(E_F)$, with χ_{Pauli} is in unit of $\text{cm}^3 \text{mol}^{-1}$ and $N(E_F)$ is in unit of states/eV f.u. for both spins directions (f.u. means formula unit) with $N(E_F) = N_{\text{band}}(E_F)(1 + \lambda_{\text{ep}})$. The band DOS $N_{\text{band}}(E_F)$ is given by an exact band-structure calculation. In the absence of electron–phonon (e–p) coupling, the bare Sommerfeld coefficient γ_0 is given by

$$\gamma_0 = \frac{\pi^2 k_B^2}{3} N_{\text{band}}(E_F) = 2.359 N_{\text{band}}(E_F). \quad (6)$$

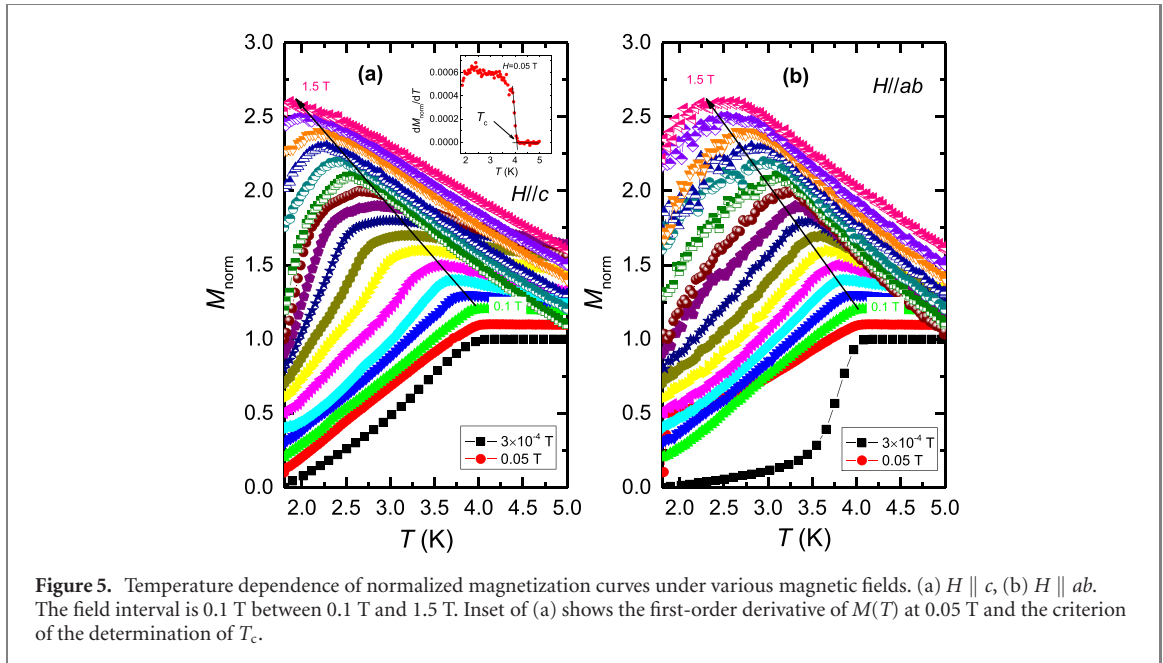
Here, γ_0 is in unit of $\text{mJ mol}^{-1} \text{K}^{-2}$. Taking the e–p coupling into account, the Sommerfeld coefficient is given by $\gamma = \gamma_0(1 + \lambda_{\text{ep}})$ with λ_{ep} is the e–p coupling constant. Combining equations (5) and (6), the χ_{Pauli} can be rewritten as

$$\chi_{\text{Pauli}} = \frac{3\mu_B^2}{\pi^2 k_B^2} \gamma = (1.370 \times 10^{-5})\gamma. \quad (7)$$

Using the estimated value $\gamma_s = 3.46 \text{ mJ mol}^{-1} \text{K}^{-2}$ (see the discussion section for details), we obtain χ_{Pauli} is $47.4 \times 10^{-6} \text{ cm}^3 \text{mol}^{-1}$. In a normal metal or a highly doped extinct semiconductor [39], the χ_{Landau} is approximately given by

$$\chi_{\text{Landau}} = -\frac{1}{3} \left(\frac{m_e}{m^*} \right)^2 \chi_{\text{Pauli}}, \quad (8)$$

where m_e and m^* are the electron mass and the effective electron mass. Adopting $m^* = 0.194m_e$ [2], we estimate $\chi_{\text{Landau}} = -419.8 \times 10^{-6} \text{ cm}^3 \text{mol}^{-1}$, showing a considerable enhancement compared to the counterpart of a normal metal. Moreover, similar to parent Bi_2Se_3 [26, 40], the $\text{Cu}_{0.09}\text{Bi}_2\text{Se}_3$ is assumed to be strongly covalent bonding in quintuple-layers with only a small ionic contribution. Since the Cu atoms are intercalated into van der Waals gap between quintuple layers, the ionic bonding is supposed to be dominant. To calculate the total core contribution, the χ_{core} values of Cu^{1+} , Bi^{3+} , Se^{2-} ions are taken from the tabulated data in reference [41], $\chi_{\text{core}}(\text{Cu}^{1+}) = -12 \times 10^{-6} \text{ cm}^3 \text{mol}^{-1}$, $\chi_{\text{core}}(\text{Bi}^{3+}) = -25 \times 10^{-6} \text{ cm}^3 \text{mol}^{-1}$, $\chi_{\text{core}}(\text{Se}^{2-}) = -48 \times 10^{-6} \text{ cm}^3 \text{mol}^{-1}$, yielding the core susceptibility per mole of $\text{Cu}_{0.09}\text{Bi}_2\text{Se}_3$ as $\chi_{\text{core}}^{\text{ionic}} = -195.1 \times 10^{-6} \text{ cm}^3 \text{mol}^{-1}$. If making use of the values of atomic core diamagnetic susceptibility calculated by the relativistic Hartree–Fock method [42] (see table 2.1 in reference [42]), $\chi_{\text{core}}(\text{Bi}) = -58.9 \times 10^{-6} \text{ cm}^3 \text{mol}^{-1}$, $\chi_{\text{core}}(\text{Se}) = -32.4 \times 10^{-6} \text{ cm}^3 \text{mol}^{-1}$, we obtain $\chi_{\text{core}}^{\text{atomic}} = -215.1 \times 10^{-6} \text{ cm}^3 \text{mol}^{-1}$. One finds that there is no significant difference between $\chi_{\text{core}}^{\text{ionic}}$ and $\chi_{\text{core}}^{\text{atomic}}$. The van Vleck susceptibility is ignored due to the absence of any ion with a shell that is one electron short of being half filled ($J = |S + L|$ with $J = 0$, the ground state is non-degenerate). Finally, one gets the sum $\chi_0^{\text{ionic}} \cong -56.8 \times 10^{-5} \text{ cm}^3 \text{mol}^{-1}$ and $\chi_0^{\text{atomic}} \cong -58.8 \times 10^{-5} \text{ cm}^3 \text{mol}^{-1}$, which is almost four times smaller than the experimental observed value $\chi_0^{\text{exp}} = -15.6 \times 10^{-5} \text{ cm}^3 \text{mol}^{-1}$ at 300 K. This may be mainly caused by two reasons. One possibility is that the absolute value of χ_{Landau} is calculated based on the reported value of m_e/m^* in higher Cu doping sample [2], which somehow results in uncertainty. Especially, the heat capacity measurement shows the m^* in $\text{Cu}_{0.29}\text{Bi}_2\text{Se}_3$ was as large as $m^* = 2.6m_e$ [43], strongly reducing the diamagnetic Landau contribution if this is the case. However, according to the quantum oscillation [2, 29, 44] and



optical spectroscopic studies [44, 45], the large electronic mass enhancement ($m^*/m_e = 0.14\text{--}0.3$) in $\text{Cu}_x\text{Bi}_2\text{Se}_3$ is not observed and thus the discrepancy from the Landau diamagnetic term seems unfavorable. The other possibility is there might be some contributions from other kinds of paramagnetic defects [30], like the Se vacancies, as proposed in CuInSe_2 compound. An exact dominant factor to explain the discrepancy between the experimental observed value and the calculated value of χ_0 needs further explorations. Regardless of the origin of the discrepancy, the total paramagnetic susceptibility could be calculated in terms of $\chi_P = \chi_{\text{Pauli}} + (\chi_0^{\text{exp}} - \chi_0^{\text{atomic}}) = 47.9 \times 10^{-5} \text{ cm}^3 \text{ mol}^{-1}$. The magnetic parameters are summarized in table 1.

3.3. Upper critical field

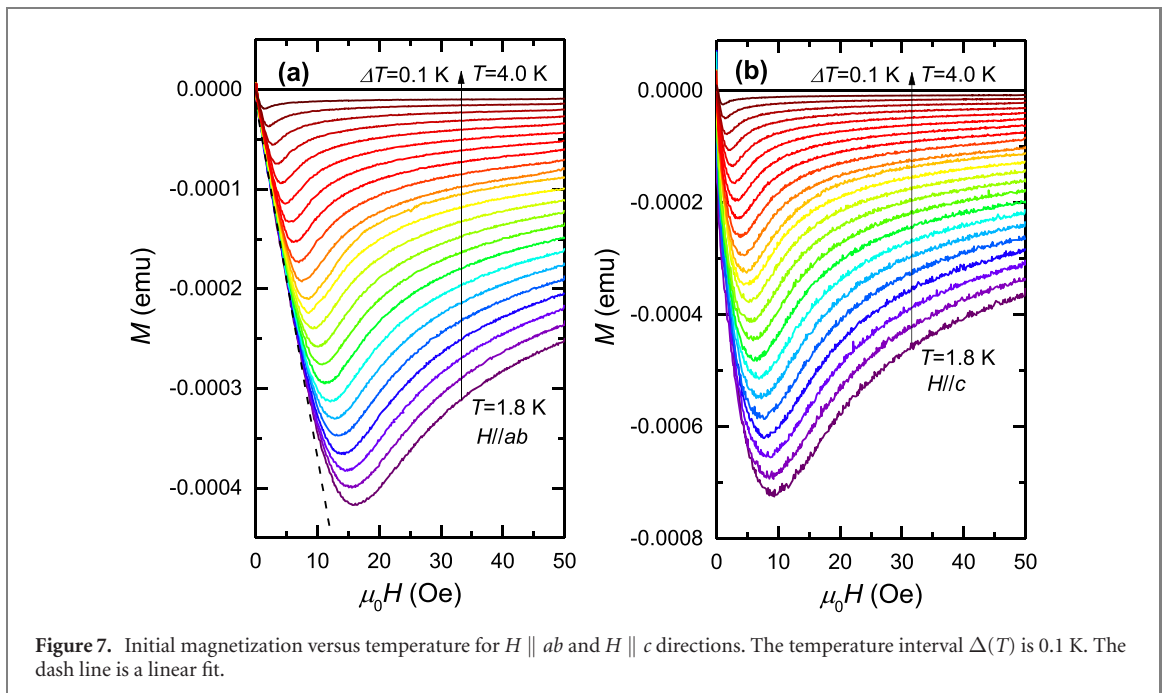
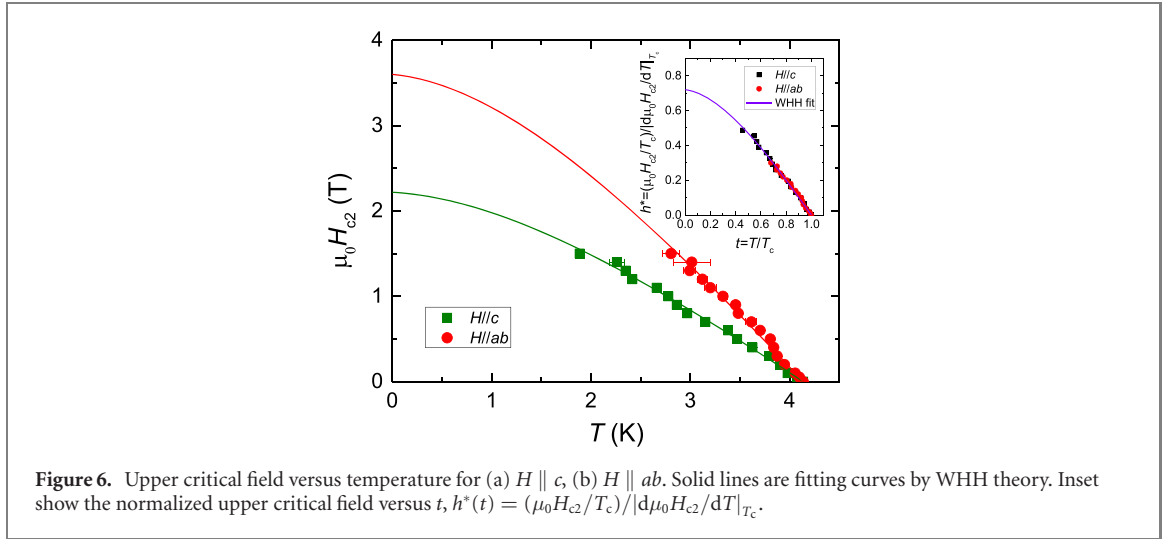
To investigate the effect of applied fields on the T_c , we measured the $M(T)$ curves under various magnetic fields. Figures 5(a) and (b) show a series of normalized $M(T)$ curves, M_{norm} , with a parallel shift of the curves for clarity. The T_c was determined by the intersection point between the extrapolation lines below and above the superconducting transition, as indicated in the inset of figure 5(a). We plot the upper critical field $\mu_0 H_{c2}^c(0)$ and $\mu_0 H_{c2}^{ab}(0)$ for $H \parallel c$ and $H \parallel ab$ in figure 6. The early reports on Bi_2Se_3 and $\text{Cu}_x\text{Bi}_2\text{Se}_3$ ($T_c \cong 3.5$ K) under high pressure indicates the absence of Pauli limiting effect and an enhancement of $\mu_0 H_{c2}^{\text{orb}}(T)$ at zero-temperature limit [46, 47]. The estimated electron mean free path l is larger than the coherence length ξ , suggesting the superconductivity in $\text{Cu}_x\text{Bi}_2\text{Se}_3$ crystals grown by melt method are in the clean limit [15, 47]. We further fit the experimental quantities $\mu_0 H_{c2}^c(T)$ and $\mu_0 H_{c2}^{ab}(T)$ by the orbital-limited formula of Werthamer–Helfand–Hohenberg (WHH) theory [48] and the data above 1.8 K agree well with the WHH prediction, as is shown in figure 6. At 0 K, it yields $\mu_0 H_{c2}^c(0) = 2.22$ T and $\mu_0 H_{c2}^{ab}(0) = 3.60$ T. Moreover, we have plotted the normalized upper critical field, $h^*(t) = (\mu_0 H_{c2}/T_c)/|d\mu_0 H_{c2}/dT|_{T_c}$, both for $H \parallel c$ and $H \parallel ab$. The two $\mu_0 H_{c2}(T)$ curves collapse onto a single universal function $h^*(t)$, as is similar to that reported by Bay *et al* [47]. Using the Ginzburg–Landau (GL) relations, we extract the $\xi_{ab}(0) = 12.18$ nm and $\xi_c(0) = 7.51$ nm at 0 K. This manifests the anisotropy ratio $\Gamma = \xi_{ab}/\xi_c = 1.62$, which is smaller than the value determined by magnetotransport measurements [15, 43]. The anisotropy may result from the in-plane nematic superconducting state (about ± 0.5 difference in Γ from $\mu_0 H_{c2}^{ab}(0)$ along x and y axis) evidenced from the high-resolution heat capacity measurements of $\text{Cu}_x\text{Bi}_2\text{Se}_3$ ($T_c \cong 3.2$ K) [49].

3.4. Lower critical field

To determine the lower critical field $\mu_0 H_{c1}$, the demagnetization effect due to the sample shape shall be taken into account. To this end, the $\mu_0 H_{c1}$ is obtained by [50]

$$\mu_0 H_{c1}(T) = \mu_0 H_p(T) / (1 + N \cdot \chi_{\text{int}}), \quad (9)$$

where $\mu_0 H_p(T)$ is the first penetration field as can be determined by the initial magnetization versus the magnetic field $M(H)$. $\chi_{\text{int}} = -1$ for a homogeneous bulk superconductor at most temperatures below T_c .



Given the non-bulk superconductivity in $\text{Cu}_{0.20}\text{Bi}_2\text{Se}_3$, we mainly focus on the $\mu_0 H_{c1}(T)$ for $H \parallel ab$ due to the small effect of demagnetization. Figures 7(a) and (b) show the initial $M(H)$ curves for $H \parallel ab$ and $H \parallel c$. The extending tails of diamagnetic signals above the minimum indicates a typical feature of the type-II superconductors.

To extract the $\mu_0 H_{c1}$, one common used criterion is assigning the deviation from the linear behavior of initial $M(H)$ as the $\mu_0 H_p^I$, designated as criterion I. Figures 8(a) and (b) show the plots of $\Delta M = M_{\text{exp}} - M_{\text{fit}}$ versus field, where the $M_{\text{fit}} = s \cdot \mu_0 H$ with s being the slope of the initial magnetization. Due to the small $\mu_0 H_{c1}$, the boundary of deviation from linear behavior is not well defined, especially for $H \parallel c$. This would bring much noise in the directly extracted $\mu_0 H_p$. Here, we also use an alternative criterion, designated as criterion II, i.e., the intersection point as $\mu_0 H_p^{II}$ from the linear fitting of ΔM slightly above the field where $\Delta M \cong 0$, as seen in figure 8(c). From these two criterions, we obtain the $\mu_0 H_{c1}$ as shown in figures 9(a) and (b). The experimental data points follow on a parabolic line, which is fitted by a GL phenomenological model as given by

$$\mu_0 H_{c1}(T) = \mu_0 H_{c1}(0) [1 - (T/T_c)^2]. \quad (10)$$

We thus obtain the $\mu_0 H_{c1}^{ab}(0) = 10.6(1)$ Oe and $\mu_0 H_{c1}^c(0) = 6.82(6)$ Oe. The smaller value of $\mu_0 H_{c1}^c$ than $\mu_0 H_{c1}^{ab}$ is attributed to the non-bulk superconductivity. If one assumes $\chi_{\text{int}} = -1$, this will yield $\mu_0 H_{c1}^{ab}(0) = 11.86$ Oe and $\mu_0 H_{c1}^c(0) = 41.50$ Oe, respectively. To calculate the GL parameter κ , we adopt a relation by

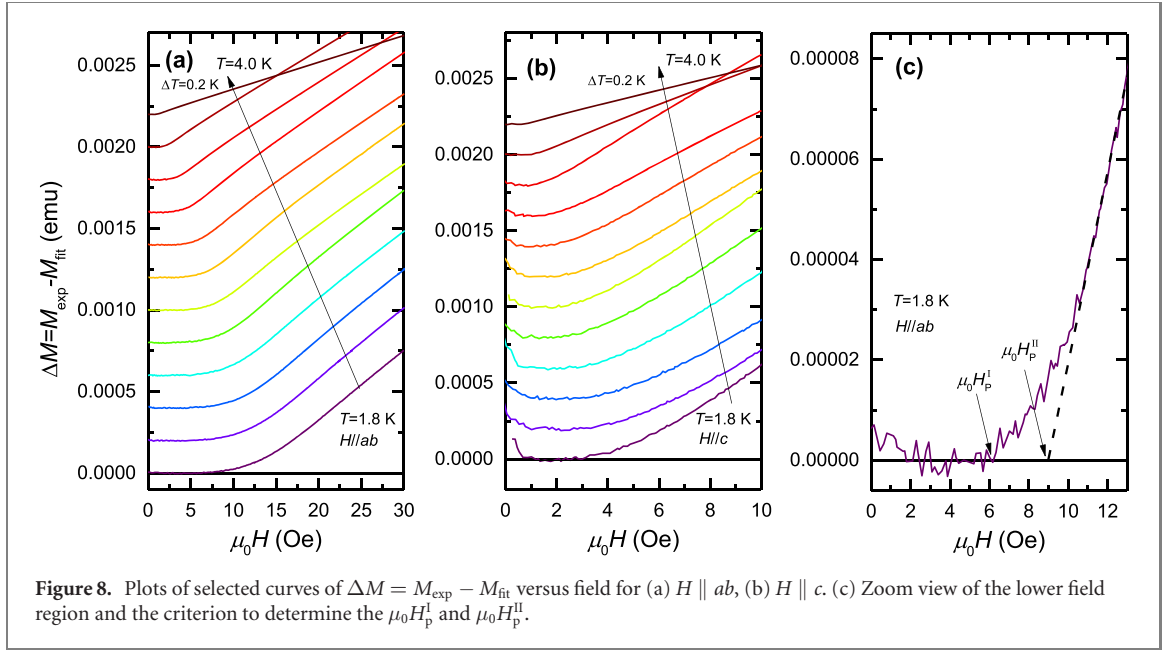


Figure 8. Plots of selected curves of $\Delta M = M_{\text{exp}} - M_{\text{fit}}$ versus field for (a) $H \parallel ab$, (b) $H \parallel c$. (c) Zoom view of the lower field region and the criterion to determine the $\mu_0 H_p^I$ and $\mu_0 H_p^{II}$.

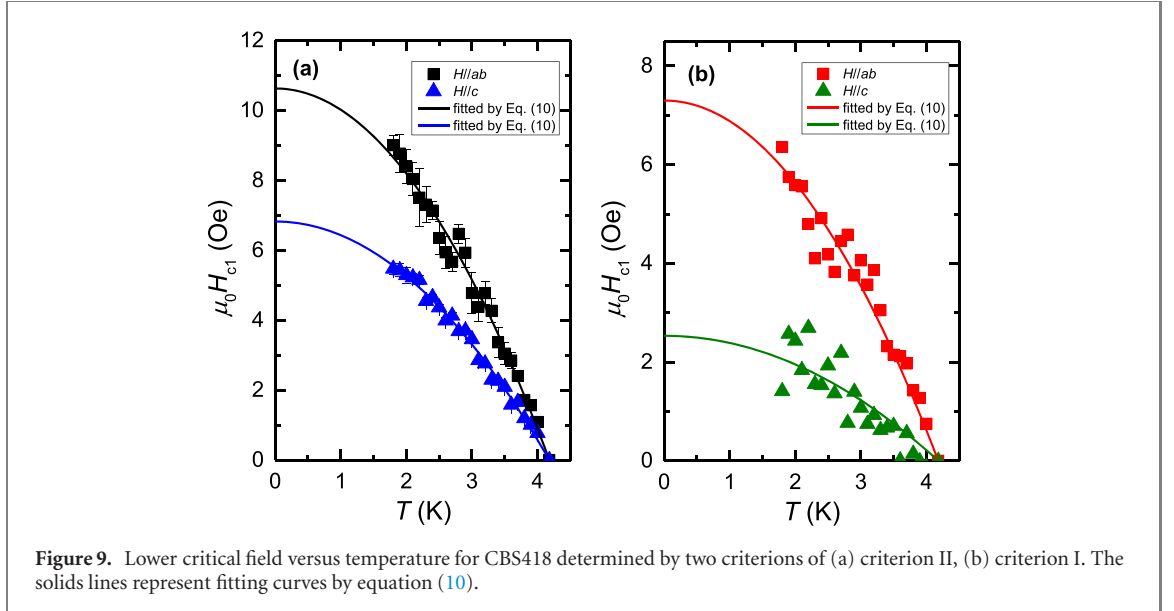


Figure 9. Lower critical field versus temperature for CBS418 determined by two criteria of (a) criterion II, (b) criterion I. The solids lines represent fitting curves by equation (10).

taking into account the vortex core energy given by [51, 52]

$$\mu_0 H_{c1}^{ab}(T) = (\Phi_0 / 4\pi \lambda_{ab} \lambda_c) (\ln \kappa_{ab} + 0.5), \quad (11)$$

$$\mu_0 H_{c2}^{ab}(T) / \mu_0 H_{c1}^{ab}(T) = 2\kappa_{ab}^2 / (\ln \kappa_{ab} + 0.5). \quad (12)$$

The κ is only weakly dependent on the temperature and the doping [52], as is the same case of Γ ($\Gamma = \lambda_c / \lambda_{ab}$) in $\text{Cu}_x\text{Bi}_2\text{Se}_3$ [15, 53]. Thus the relation $\mu_0 H_{c1}^{ab}(T) \propto 1/\lambda_{ab} \lambda_c \propto 1/\lambda_{ab}^2$ is a good approximation. For anisotropic superconductors, the κ is defined as $\kappa_{ab} = \sqrt{\lambda_{ab} \lambda_c / (\xi_{ab} \xi_c)} = \lambda_{ab} / \xi_c$ and $\kappa_c = \lambda_{ab} / \xi_{ab}$. Using equations (11) and (12) with $\mu_0 H_{c1}^{ab,I}(0) = 6.0(3)$ Oe and $\mu_0 H_{c1}^{ab,II}(0) = 9.7(3)$ Oe obtained in the clean limit (see next section), we obtain $\kappa_{ab}^I = 126.58$ and $\kappa_{ab}^{II} = 97.05$, respectively. The value of κ_{ab}^I is very close to the early report (~ 128) [43]. Hereafter, we mainly use this value to derive the related physical parameters as following. The penetration depth at 0 K are $\lambda_{ab}^I = 1541.57$ nm and $\lambda_c^I = 2499.84$ nm, yielding the averaged value $\lambda_{av}^I = (\lambda_{ab}^I \lambda_c^I)^{1/3} = 1811.12$ nm. Matano *et al* reported $\lambda_{ab} = 1038$ nm and $\lambda_c = 1612$ nm at 0.5 K in $\text{Cu}_{0.3}\text{Bi}_2\text{Se}_3$ [54]. Using muon spin rotation (μSR) spectroscopy, Krieger *et al* obtained the effective penetration depth $\lambda_{\text{eff}} \sim 1600$ nm [55]. The penetration depth at 0 K we gain is in good line with the reported results. The thermodynamic critical field is further determined by

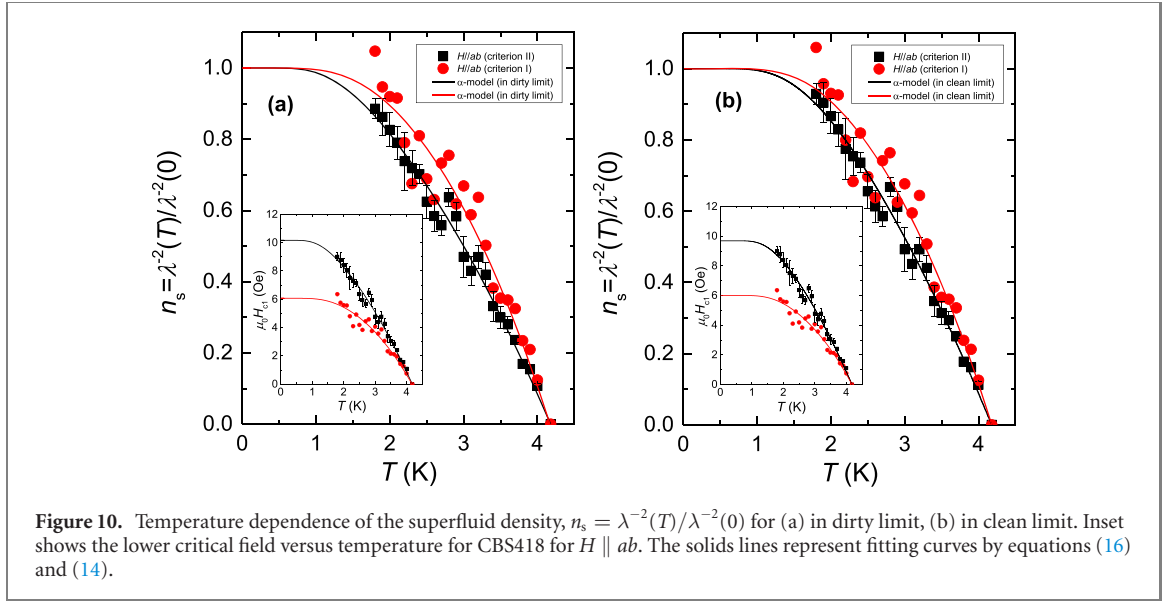


Table 2. Physical parameters derived from the analysis of the superconducting transitions in $M(T)$ under magnetic field and initial $M(H)$.

Sample	Properties	Units	Values	Remarks
CBS418	T_c	K	4.18	
	$\mu_0 H_{c1}^{ab,II}$	Oe	10.6(1)	GL empirical formula, fitted by equation (10)
	$\mu_0 H_{c1}^{c,II}$	Oe	6.82(6)	
	$\mu_0 H_{c1}^{ab,I}$	Oe	10.2(4)	In dirty limit, fitted by equation (16)
	$\mu_0 H_{c1}^{ab,I}$	Oe	6.1(3)	
	$\mu_0 H_{c1}^{ab,II}$	Oe	9.7(3)	In clean limit, fitted by equation (14)
	$\mu_0 H_{c1}^{ab,I}$	Oe	6.0(3)	
	α_{ab}^{II}		1.26(10)	In dirty limit, equation (16)
	α_{ab}^I		1.7(2)	
	α_{ab}^{II}		1.759	In clean limit, equation (14)
	α_{ab}^I		2.029	
	Δ_0^I	meV	0.61(7)	In dirty limit, equation (16)
	Δ_0^I	meV	0.73	In clean limit, equation (14)
	$\mu_0 H_{c2}^{ab}$	T	3.60	
	$\mu_0 H_{c2}^c$	T	2.22	
	$d\mu_0 H_{c2}^{ab}/dT$	T K ⁻¹	1.20(4)	
	$d\mu_0 H_{c2}^c/dT$	T K ⁻¹	0.73(3)	
	$\mu_0 H_c$	Oe	211.23	
	Γ		1.62	
	$\xi_{ab}(0)$	nm	12.18	
$\xi_c(0)$	nm	9.56		
κ_{ab}^{II}		97.05		
κ_{ab}^I		126.58		
λ_{ab}^I	nm	1541.57		
λ_{eff}	nm	~1600	[55]	
$\mu_0 H_{c2}^{ab}$	T	3.02		
$\mu_0 H_{c2}^c$	T	1.71		
$\mu_0 H_{c1}^{ab}$	Oe	4.5	[43]	
$\mu_0 H_c$	Oe	~167		
κ_{ab}^I		~128		
Δ_0^I	meV	0.52		
α_{ab}^I		1.9		
Γ		1.77		

$\mu_0 H_c = \sqrt{\mu_0 H_{c2}^{ab} \mu_0 H_{c1}^{ab,I} / \ln \kappa_{ab}^I}$, which yields 211.23 Oe at 0 K. This value is close to the reported value 167 Oe in $Cu_x Bi_2 Se_3$ prepared by an electrochemical technique [43].

3.5. Superfluid density

To study the temperature dependence of the superfluid density $n_s(T)$, we have analyzed the $\mu_0 H_{c1}(T)$ extracted in criterion I. The $n_s(T)$ is related to the λ as well as equivalently the $\mu_0 H_{c1}$, which is

given by [56, 57]

$$n_s(T) = \frac{\lambda^{-2}(T)}{\lambda^{-2}(0)} = \frac{\mu_0 H_{c1}(T)}{\mu_0 H_{c1}(0)}. \quad (13)$$

For an isotropic BCS superconductor in the clean limit, the $n_s(T)$ is given by [58]

$$n_s(T) = 1 - 2 \int_{\Delta}^{\infty} dE \left(-\frac{\partial f(E)}{\partial E} \right) \frac{E}{\sqrt{E^2 - \Delta^2(T)}}, \quad (14)$$

where $f(E) = (1 + e^{E/k_B T})^{-1}$ is Fermi distribution function, $\Delta(T)$ is the superconducting gap function, and the quasiparticle DOS is $N(E) = \frac{E}{\sqrt{E^2 - \Delta^2(T)}}$. In a good approximation, the gap function versus the temperature can be expressed as [58]

$$\Delta(T) = \Delta_0 \tanh \left\{ 1.82 [1.018(T_c/T - 1)]^{0.51} \right\}, \quad (15)$$

where Δ_0 is the energy gap at zero temperature. According to the α model [59], the quantity $\alpha \equiv \Delta_0/k_B T_c$ is treated as an adjustable parameter in equation (15), and the BCS value in weak coupling limit is $\alpha_{\text{BCS}} = 1.764$ [60]. In the dirty limit [43, 57], the $n_s(T)$ is given by

$$n_s(T) = \frac{\Delta(T)}{\Delta_0} \tanh \left(\frac{\Delta(T)}{2k_B T} \right). \quad (16)$$

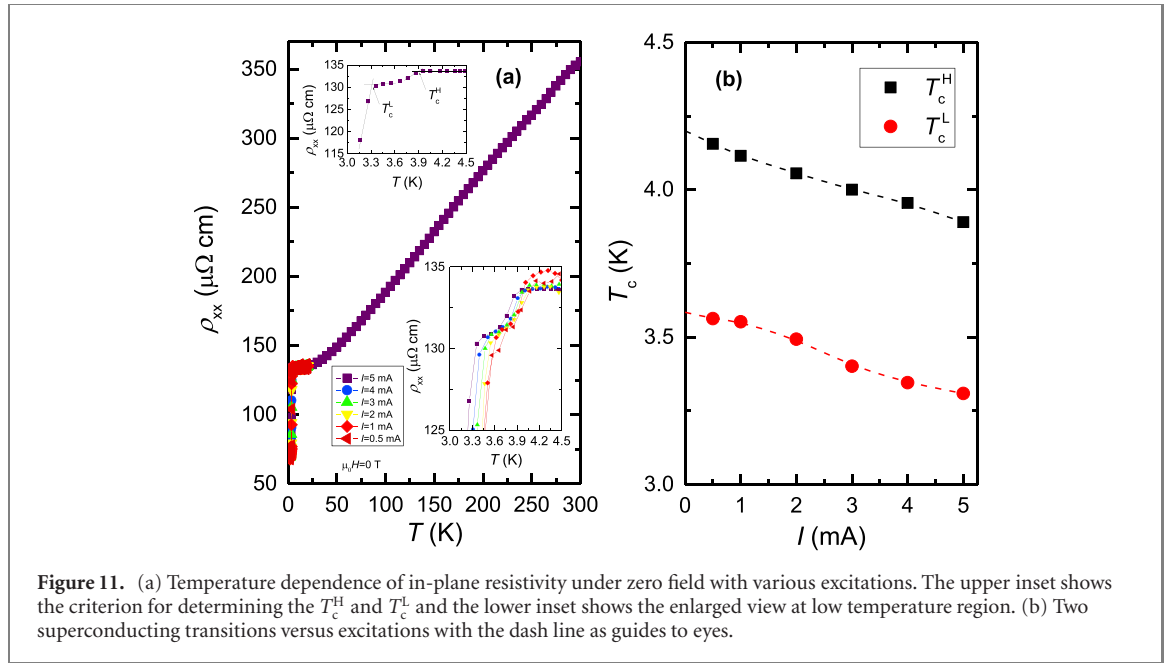
To find the difference of fitting parameters between the directly determined $\mu_0 H_{c1}^{ab,1}(T)$ (criterion I) and extrapolated $\mu_0 H_{c1}^{ab,II}(T)$ (criterion II), we plot the $\mu_0 H_{c1}(T)$ for $H \parallel ab$ in figure 10. The fitted $\mu_0 H_{c1}(T)$ curves by equations (14) and (16) are presented in insets of figure 10. The $n_s(T)$ is obtained by normalizing $\mu_0 H_{c1}(T)$. We find that while the values of $\mu_0 H_{c1}$ for criterion II in the dirty limit are slightly larger than those obtained by criterion I in the clean limit, the difference between the values of α derived from two criterions is more than 20%. Independent of the fitting strategy, the obtained α^{II} is always smaller than α^I , indicating the criterion for determination of $\mu_0 H_{c1}$ has strong influence on the magnitude of Δ_0 , i.e., the pairing strength. Here, we use the criterion I to evaluate the superconducting critical parameters. Moreover, the previous reports on $\text{Cu}_{0.10}\text{Bi}_2\text{Se}_3$ indicates the superconducting state is in the clean limit [15], which also holds here. We obtain $\alpha^I = 2.029 \pm 0.124$, suggesting $\text{Cu}_{0.09}\text{Bi}_2\text{Se}_3$ is a strong-coupling superconductor. Our result from lower critical field measurements is in line with the conclusion as inferred from the specific heat experiment in $\text{Cu}_{0.29}\text{Bi}_2\text{Se}_3$ ($\alpha = 1.9$) [43]. The physical parameters obtained in this work and from literatures are summarized in table 2.

3.6. Electrical transport properties in superconducting and normal states

To reduce the effect of inhomogeneity, we have measured a smaller piece cleaved from the bigger one used for the magnetic susceptibility measurement. Figure 11(a) shows the temperature dependence of the in-plane resistivity $\rho_{xx}(T)$ under zero field. Different magnitudes of excitations were applied to examine whether the superconductivity is robust or filamentary. As seen in figure 11(a), we clearly observe there are two superconducting transitions with the higher one (T_c^H) and the lower one (T_c^L), similar to the magnetic susceptibility measurements. This double T_c phenomenon is reminiscent of the well-known intercalated iron-selenides superconductor $\text{M}_x\text{Fe}_{2-y}\text{Se}_2$ ($M = \text{K}, \text{Rb}, \text{Tl}$) [61–63]. Actually, two systems share additional common features such as the non-bulk superconducting phase and the intercalation induced superconductivity. Interestingly, by applying high pressure [64], Sun *et al* discovered the reemergence of superconducting phase with a higher T_c up to 48 K in $\text{M}_x\text{Fe}_{2-y}\text{Se}_2$. This high-pressure phase might be the minority phase as observed in early reports at ambient condition [61–63]. In this context, it is worth exploring whether the reemergent superconductivity with a higher T_c exists in $\text{Cu}_x\text{Bi}_2\text{Se}_3$. Recently, Zhou *et al* reported the pressure-induced reemergent superconductivity with $T_c = 3.6$ K at 6 GPa in its cousin material $\text{Sr}_{0.065}\text{Bi}_2\text{Se}_3$ [65]. As seen in figure 11(a), by applying different excitations, T_c^H is still observable up to 5 mA, indicating the robust superconductivity. In figure 11(b), we plot the current dependence of the two T_c values. By extrapolation to zero current limit, we identify two superconducting transitions occur at around 4.2 K and 3.6 K, which are in consistent with the magnetic susceptibility measurements.

Furthermore, we evaluate the l of CBS418 sample, which is critical to discern whether the specimen is in the clean or the dirty limit. To evaluate this issue, we employ the slopes of upper critical field $d\mu_0 H_{c2}/dT$ near T_c [47, 66], Sommerfeld coefficient γ , residual resistivity ρ_0 . The relation between γ and the $\mu_0 H_c$ can be found in the discussion section. In the dirty limit [66], the initial slope $d\mu_0 H_{c2}/dT|_{T_c}$ at T_c is given by

$$d\mu_0 H_{c2}/dT|_{T_c} = -4.48 \times 10^4 \gamma \rho_0, \quad (17)$$



where the $d\mu_0 H_{c2}/dT|_{T_c}$ is in unit of Oe K^{-1} , γ is in unit of $\text{erg cm}^{-3} K^{-2}$ and ρ_0 is in unit of $\Omega \text{ cm}$. Our calculation shows $d\mu_0 H_{c2}/dT|_{T_c} = 0.25 \text{ T K}^{-1}$, much smaller than the experimental values $d\mu_0 H_{c2}^{ab}/dT|_{T_c} = 1.20 \text{ T K}^{-1}$ and $d\mu_0 H_{c2}^c/dT|_{T_c} = 0.73 \text{ T K}^{-1}$. This suggests that the sample is not in the dirty limit.

In the clean limit [66], the l can be calculated by the following relation:

$$l = 1.27 \times 10^4 \left[\rho_0 \left(\frac{9.55 \times 10^{24} \gamma^2 T_c}{|d\mu_0 H_{c2}/dT|_{T_c}} \right)^{1/2} \right]^{-1}, \quad (18)$$

where l is in unit of cm. For $H \parallel ab$ and $H \parallel c$, we obtain $l_{ab}(l_c) = 39.86(31.09) \text{ nm}$, which are larger than the $\xi_{ab}(0)$ and $\xi_c(0)$, indicating our CBS418 sample is in the clean limit. Taking the $k_F^x = 0.97 \text{ nm}^{-1}$ [2], we further estimate $k_F l \cong 39$, which is used as the quantity for parametrizing disorders [14, 53]. The value of $k_F l$ is close to the lower critical Cu doping level for inducing superconductivity as prepared by electrochemical synthesis route [18], implying the CBS418 sample is weakly disordered. This may be important for observing a higher T_c since the strong disorders can suppress the T_c [14, 53].

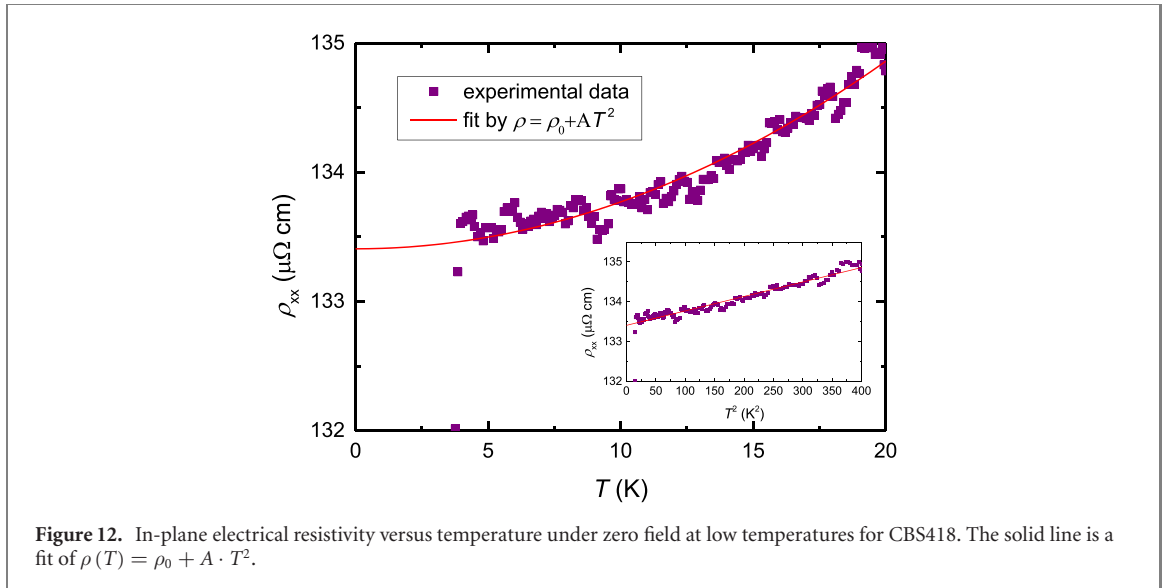
3.7. Discussion

To find the behind reason why T_c increases to 4.18 K in the CBS418 crystal, it will be helpful to estimate the DOS from the $\mu_0 H_{c2}$ and the $\mu_0 H_c$. Due to the difficulty of measuring the heat capacity jump in non-bulk superconducting $\text{Cu}_x\text{Bi}_2\text{Se}_3$, we here indirectly estimate the electronic coefficient and the DOS at E_F by the relation [67]

$$\gamma_s = \mu_0 H_c^2(0) / 2\pi T_c^2 = \frac{1}{3} \pi^2 k_B^2 N(E_F), \quad (19)$$

where γ_s is the electronic Sommerfeld coefficient. Using the parameters determined before, we obtain $\gamma_s = 3.46 \text{ mJ mol}^{-1} K^{-2}$ and $N(E_F) = 3.76 \text{ states/eV atoms spin}^{-1} \text{ per f.u.}$, much larger than those of ambient $\text{Cu}_{0.29}\text{Bi}_2\text{Se}_3$ obtained from the specific heat measurement [43]. We infer the enhancement of e-p interactions can account for the large DOS.

Before applying the BCS theory to further discuss the unusual 'high T_c ' for $\text{Cu}_{0.09}\text{Bi}_2\text{Se}_3$, we have examined if the adiabatic limit satisfies or not in $\text{Cu}_x\text{Bi}_2\text{Se}_3$. The BCS solution is only a good description for the systems in the adiabatic limit [68, 69], which requires the phonon energy $\hbar\omega$ must be much smaller than the carrier relaxation rate \hbar/τ , namely, $\omega\tau \ll 1$. To make such an estimation, taking the highest phonon frequency A_{1g}^2 mode 175.4 cm^{-1} at 3 K for Bi_2Se_3 [70] and the scattering time $\tau = 5.2 \times 10^{-14} \text{ s}$ for $\text{Cu}_{0.25}\text{Bi}_2\text{Se}_3$ [2], we obtain $\omega\tau = 0.27$ as an upper bound. This indicates the $\text{Cu}_x\text{Bi}_2\text{Se}_3$ is close to violate the adiabatic limit for optical branch but is satisfied for acoustic branches due to its lower frequency in the long-wavelength limit. A brief discussion on the enhancement of T_c within BCS theory can be found in supplementary material stacks.iop.org/NJP/22/053026/mmedia. Nevertheless, according to our calculation of E_F for $\text{Cu}_x\text{Bi}_2\text{Se}_3$ in the following, the Debye frequency (ω_D) [43] is actually comparable with the order of the E_F , suggesting the antiadiabatic effect needs to be considered. If the optical phonons are at play in



mediating superconductivity in $\text{Cu}_x\text{Bi}_2\text{Se}_3$, the standard BCS theory has to be modified by including the antiadiabatic effect [68, 71, 72]. Theoretically, Wan and Savrasov showed the phonon dispersions of electron-doped Bi_2Se_3 has an unusual large linewidth for both highest optical and acoustic phonons along Γ -Z direction [27]. In the antiadiabatic limit, the enhanced e-p interaction by optical phonons may be crucial generating the unusual ‘high T_c ’ for $\text{Cu}_{0.09}\text{Bi}_2\text{Se}_3$ although the acoustic phonon-mediated exotic superconductivity cannot be fully ruled out [73]. In this context, further experimental and theoretical efforts shall be made to clarify the unusual ‘high T_c ’ for Bi_2Se_3 -based superconductors.

According to the discussion in supplementary material, the electron–electron (e–e) scattering dominates over the e–p scattering at low temperatures for $\text{Cu}_x\text{Bi}_2\text{Se}_3$. Actually, the evaluated values of $k_{\text{F}}l > 1/2\pi \sim 0.16$ for various Cu doping range ($0.11 \leq x \leq 0.50$) and $k_{\text{F}}l \gg 0.16$ in CBS418 sample assures the Fermi-liquid description is appropriate [53, 74]. To further estimate the Kadowaki–Woods (KW) ratio [75], A/γ^2 , being a measure of the magnitude of the e–e correlation, we fit the $\rho(T)$ data using the simple formula, $\rho(T) = \rho_0 + A \cdot T^2$, to extract the e–e scattering contribution. As shown in figure 12, the fitting yields $\rho_0 = 133.41(1) \mu\Omega \text{ cm}$ and $A = 0.00363(7) \mu\Omega \text{ cm K}^{-2}$. For many heavy-fermion compounds [75], the KW ratio is found to follow a universal value, $A/\gamma^2 = a_0 \approx 1.0 \times 10^{-5} \mu\Omega \text{ cm mol}^2 \text{ K}^2 \text{ mJ}^{-2}$, while for a lot of transition metals [76], $A/\gamma^2 \approx 4.0 \times 10^{-7} \mu\Omega \text{ cm mol}^2 \text{ K}^2 \text{ mJ}^{-2} = 0.04a_0$. Using the values of $\gamma_s = 3.46 \text{ mJ mol}^{-1} \text{ K}^{-2}$, we obtain $A/\gamma^2 = 30.3a_0$. At higher Cu doping region, a larger KW ratio would be expected according to Kriener *et al*’s electrical transport and specific heat results of $\text{Cu}_{0.29}\text{Bi}_2\text{Se}_3$ (a rough estimation yields $A/\gamma^2 \sim 180a_0$) [43]. We plot the KW ratios for various compounds in figure 13. In a single-band quasi-2D metal [77, 78], the coefficient A is given by

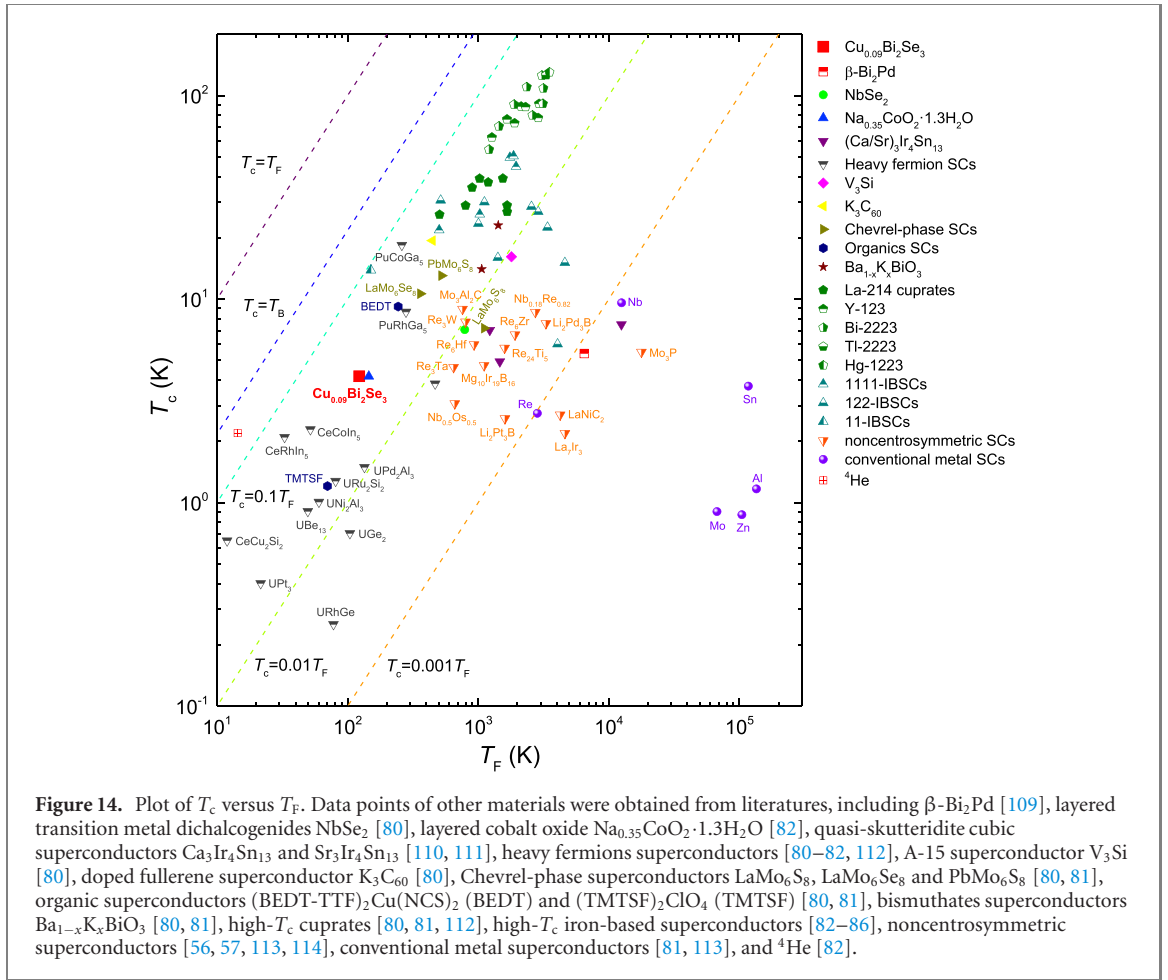
$$A = \left(\frac{8\pi^3 a c k_{\text{B}}^2}{e^2 \hbar^3} \right) \left(\frac{m^*}{k_{\text{F}}^3} \right). \quad (20)$$

Taking the values of $a = 4.143 \text{ \AA}$ and $c = 28.636 \text{ \AA}$ for Bi_2Se_3 [17], $m^* = 0.194m_e$ and $k_{\text{F}}^x(k_{\text{F}}^z) = 0.97(1.26) \text{ nm}^{-1}$ [2], we obtain $A^x(A^z) = 0.00638(0.00290) \mu\Omega \text{ cm K}^{-2}$, which is consistent with the fitted value. This indicates the quasi-2D conduction feature in $\text{Cu}_x\text{Bi}_2\text{Se}_3$, as is expected from its layered crystal structure. Thus the 2D Fermi liquid dominates at low temperatures. From the analysis mentioned above, we infer that the large KW ratio may either result from the anisotropy as proposed in Sr_2RuO_4 [79] or the proximity to the charge density instability [7].

To classify the unconventional and conventional superconductors, Uemura *et al* plotted the T_c versus the effective Fermi temperature T_{F} [80, 81]. For the heavy-fermion, high- T_c cuprates, organics, doped fullerene and other unconventional superconductors, the ratio T_c/T_{F} falls within the range of $0.01 \leq T_c/T_{\text{F}} \leq 0.1$. Recently, it is reported that the ratios T_c/T_{F} for iron-based superconductors also lie in the similar range [82–86]. For the 3D superconducting systems in the clean limit [80, 81], the T_{F} can be calculated by using the equation

$$k_{\text{B}}T_{\text{F}} = \frac{\hbar^2 (3\pi^2 n)^{2/3}}{2 m^*}. \quad (21)$$

While in the 2D case, one can convert the volume carrier density n into an areal density on the conducting planes, $n^{2\text{D}} = n \cdot d_{\text{int}}$, where d_{int} is the average inter-plane distance. Therefore, one can obtain the relation

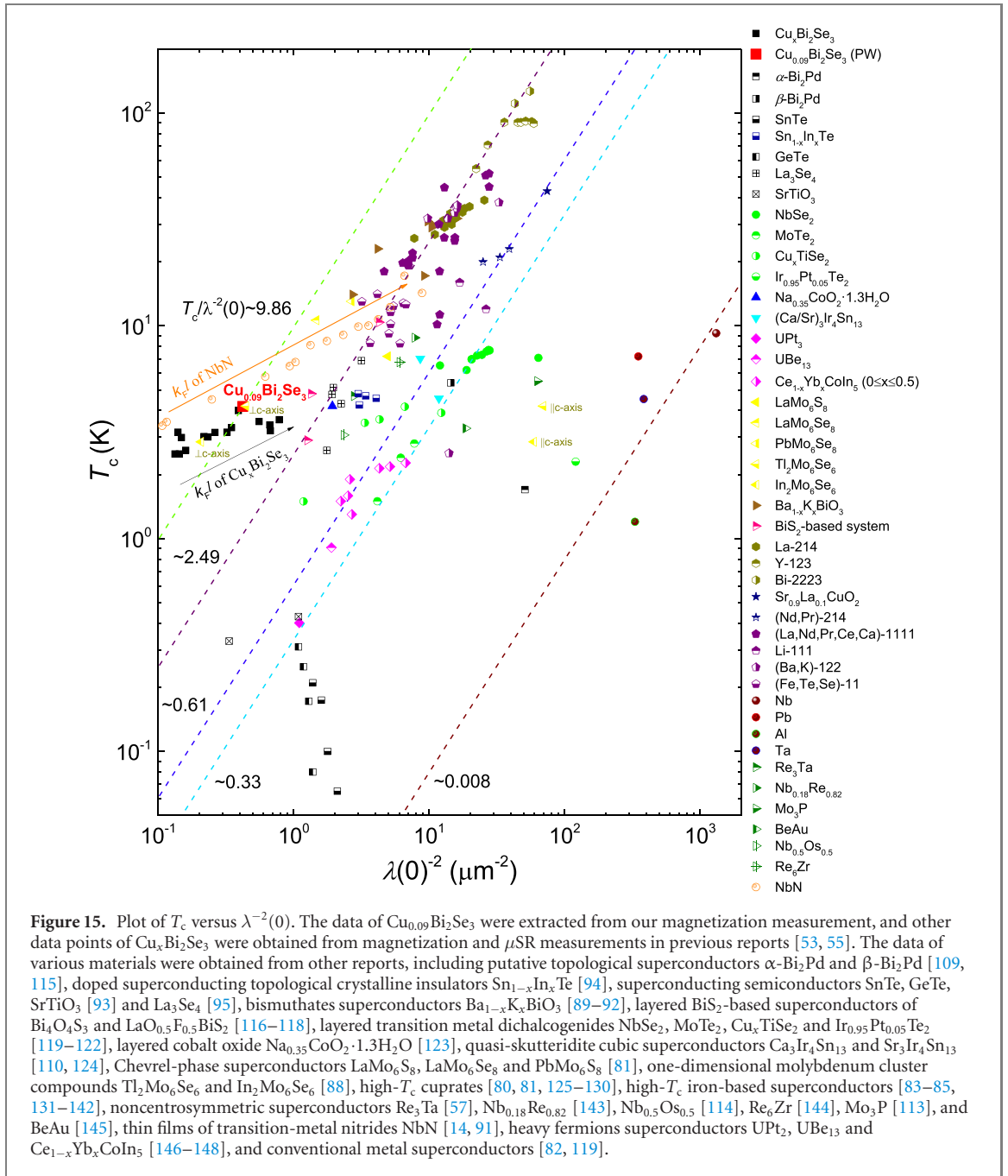


et al [53]. With increasing $k_F l$, although the T_c value increases, the ratio $T_c/\lambda^{-2}(0)$ tends to decrease but is still larger than those of high- T_c cuprates and iron-based superconductors. The large ratio $T_c/\lambda^{-2}(0)$ was also observed in LaMo₆Se₈ [81] and in one-dimensional molybdenum cluster compounds Tl₂Mo₆Se₆ and In₂Mo₆Se₆ [88], which may arise from the considerable anisotropy or the proximity to CDW instability. Also, the Ba_{1-x}K_xBiO₃ with maximum $T_c = 34$ K ($x = 0.35$) derives from a diamagnetic semiconductor BaBiO₃ with the CDW [10], and the superconductivity occurs by suppressing the CDW through doping and accompanying a cubic–tetragonal structural phase transition. The large ratio $T_c/\lambda^{-2}(0)$ was also reported in Ba_{1-x}K_xBiO₃ [89–92].

Another factor to enhance the $T_c/\lambda^{-2}(0)$ is the chemical doping, as demonstrated in SnTe. Before In doping, SnTe is a superconducting narrow-band semiconductor with a low carrier density (n_p up to 2×10^{21} cm⁻³, $T_c = 0.21$ K) and the $T_c/\lambda^{-2}(0)$ value is 0.03–0.15 [93]. However, the T_c can be greatly improved to 4.5 K by In doping despite the decrease of $\lambda(0)$ compared to SnTe [94]. Interestingly, the $T_c/\lambda^{-2}(0)$ for Sn_{1-x}In_xTe is enhanced to the range of 1.12–1.60, implying the unconventional superconductivity. Lastly, it is meaningful to compare with other unusual superconducting semiconductors such as SrTiO₃ [93] and La₃Se₄ [95]. The latter one has a relatively high T_c largely depending on the electron carrier density ($n_e = 1.2$ to 3.67×10^{21} cm⁻³, $T_c = 2.60$ –6.86 K). Both materials undergo a lattice instability at low temperatures. For instance, La₃Se₄ has a lattice instability at 60 K, where a structure distortion from cubic to tetragonal occurs [96], while the same crystallographic change takes place at 110 K in SrTiO₃ [93]. It implies the higher T_c and larger $T_c/\lambda^{-2}(0)$ shall be relevant to this lattice distortion. Altogether, the route of tuning the disorders or the chemical doping in semiconductors can be adopted to search more exotic superconductors.

Experimentally, the small negative susceptibility in Cu_{0.09}Bi₂Se₃ indicates the very weak magnetic correlations. One can further estimate the decrease of DOS from the $\chi(T)$ by the following relation:

$$\Delta\gamma = \Delta\chi \cdot (\pi k_B)^2 / (\mu_0 \mu_{\text{eff}}^2). \quad (25)$$



The change of the χ across the charge density anomaly transition can be calculated by the following relation:

$$\Delta\chi_{\text{Pauli}} = (1.370 \times 10^{-5}) \times 2.359\Delta N(E_F) = (3.23183 \times 10^{-5})\Delta N(E_F), \quad (26)$$

which yields $\Delta N(E_F) = 0.07299$ states per eV f.u. for $H \parallel c$ and 0.00616 states per eV f.u. for $H \parallel ab$. This indicates the strong anisotropy of the FS. The previous results from the ARPES [29] and quantum oscillations [97] showed that the $\text{Cu}_x\text{Bi}_2\text{Se}_3$ has a 2D cylinder FS with high carrier density. This potentially brings the FS nesting. As is well known, the FS nesting could be a crucial ingredient for the CDW [98], which again enhances the e–p interactions. In a previous theoretical work, Wan and Savrasov proposed there existed a strong FS nesting at small wave vectors \mathbf{q} along the $\Gamma(000) - Z(\pi\pi\pi)$ direction in $\text{Cu}_x\text{Bi}_2\text{Se}_3$ [27], which could greatly enhance the e–p coupling constant λ . Actually, with increasing the carrier density, the FS exhibits a tendency to become a 2D-like one [29]. In principle, the FS nesting can assist the formation of CDW state [98]. However, the strong spin–orbit coupling and/or the e–p coupling shall also be considered for the origin of the charge density anomaly in CBS418 [8, 99]. In any case, the nature of the observed charge density anomaly needs to be further clarified, which is believed to relate to the ‘high- T_c ’ superconductivity in doped topological insulators.

Table 3. Electronic properties of CBS418 sample in present work (PW).

Properties	Units	Values	References
m	m_e	0.194	[2]
k_F^x	nm^{-1}	0.97	[2]
k_F^z/k_F^x		1.3	[2]
l_{ab}	nm	39.86	PW
l_c	nm	31.09	PW
$k_F l$		$\cong 39$	PW, [2]
A_{exp}	$\mu\Omega \text{ cm K}^{-2}$	0.003 63(7)	PW
A_{cal}^x	$\mu\Omega \text{ cm K}^{-2}$	0.006 38	PW
A_{cal}^z	$\mu\Omega \text{ cm K}^{-2}$	0.002 90	PW
T_F^{2D}	K	122.89	PW, [2]
T_c/T_F^{2D}		0.034	PW
γ_s	$\text{mJ mol}^{-1} \text{ K}^{-2}$	3.46	PW
$N(E_F)$	states/eV atoms spin ⁻¹ per f.u.	3.76	PW
γ_s	$\text{mJ mol}^{-1} \text{ K}^{-2}$	1.95	[43]
$N(E_F)$	states/eV atoms spin ⁻¹ per f.u.	1.34	[43]
$T_c/\lambda_{ab}^{-2}(0)$	$\text{K } \mu\text{m}^{-2}$	9.94	PW
$T_c/\lambda_{\text{eff}}^{-2}(0)$	$\text{K } \mu\text{m}^{-2}$	10.24	[55]

4. Summary and conclusions

To summarize, we report the investigations of the physical properties of $\text{Cu}_{0.09}\text{Bi}_2\text{Se}_3$ single crystal with $T_c^{\text{onset}} = 4.18$ K. According to the magnetic susceptibility, a charge density anomaly at 96 K was observed. This leads to a conjecture of the possible coexistence of charge density wave and superconductivity in Cu doped Bi_2Se_3 topological insulator. We determined the $\mu_0 H_{c2}(T)$ and $\mu_0 H_{c1}(T)$ from the magnetization curves for $\text{Cu}_{0.09}\text{Bi}_2\text{Se}_3$. In the clean limit, the $\mu_0 H_{c1}(0)$ was extracted to be 6.0 Oe for $H \parallel ab$. The experimental energy gap ratio was $\Delta_0/k_B T_c = 2.029 \pm 0.124$, indicating it is a strong-coupling superconductor. From electrical transport measurements, the 2D Fermi liquid behavior is found at low temperature and a high Kadowaki–Woods ratio is determined to be $A/\gamma^2 = 30.3a_0$. Furthermore, we revealed an unprecedented high ratio $T_c/\lambda^{-2}(0) \cong 9.86$ with $\lambda_{ab}(0) = 1541.57$ nm as well as a high ratio of $T_c/T_F^{2D} = 0.034$ as comparable to those of high- T_c cuprates and iron-based superconductors. These results demonstrate the unconventional superconducting mechanism in $\text{Cu}_{0.09}\text{Bi}_2\text{Se}_3$ according to Uemura's regime. Finally, we propose the enhanced T_c up to 4.18 K results from the increased density of states at E_F and the strong electron–phonon interaction induced by the charge density instability. Our results suggest the higher T_c in $\text{Cu}_x\text{Bi}_2\text{Se}_3$ could be further achieved by gating-technique or high pressure technique, as realized in iron–selenides superconductors.

Acknowledgments

This work is supported by National Natural Science Foundation of China (Grant Nos. 11804011, 11474211). MTL also acknowledges the support of facilities for performing partial characterizations on the samples in MPI-FKF. WLY is appreciative of support from the start-up fund of Nanjing University of Aeronautics and Astronautics.

ORCID iDs

Yifei Fang  <https://orcid.org/0000-0001-5702-9005>

Wen-Long You  <https://orcid.org/0000-0003-1388-3861>

Mingtao Li  <https://orcid.org/0000-0003-1594-8008>

References

- [1] Hor Y S, Williams A J, Checkelsky J G, Roushan P, Seo J, Xu Q, Zandbergen H W, Yazdani A, Ong N P and Cava R J 2010 *Phys. Rev. Lett.* **104** 057001
- [2] Lawson B J, Hor Y S and Li L 2012 *Phys. Rev. Lett.* **109** 226406
- [3] Cohen M L 1969 *Superconductivity* ed R D Parks (New York: Marcel Dekker) vol 1
- [4] Schooley J F, Hosler W R and Cohen M L 1964 *Phys. Rev. Lett.* **12** 474
- [5] Hein R A, Gibson J W, Mazelsky R, Miller R C and Hulm J K 1964 *Phys. Rev. Lett.* **12** 320
- [6] Hein R A and Meijer P H E 1969 *Phys. Rev.* **179** 497

- [7] Morosan E, Zandbergen H W, Dennis B S, Bos J W G, Onose Y, Klimczuk T, Ramirez A P, Ong N P and Cava R J 2006 *Nat. Phys.* **2** 544
- [8] Gruner T, Jang D, Huesges Z, Cardoso-Gil R, Fecher G H, Koza M M, Stockert O, Mackenzie A P, Brando M and Geibel C 2017 *Nat. Phys.* **13** 967
- [9] Klintberg L E, Goh S K, Alireza P L, Saines P J, Tompsett D A, Logg P W, Yang J, Chen B, Yoshimura K and Grosche F M 2012 *Phys. Rev. Lett.* **109** 237008
- [10] Sleight A W 2015 *Physica C* **514** 152
- [11] Keimer B, Kivelson S A, Norman M R, Uchida S and Zaanen J 2015 *Nature* **518** 179
- [12] Dai P, Hu J and Dagotto E 2012 *Nat. Phys.* **8** 709
- [13] Morosan E, Natelson D, Nevidomskyy A H and Si Q 2012 *Adv. Mater.* **24** 4896
- [14] Mondal M, Kamlapure A, Chand M, Saraswat G, Kumar S, Jesudasan J, Benfatto L, Tripathi V and Raychaudhuri P 2011 *Phys. Rev. Lett.* **106** 047001
- [15] Li M T, Fang Y F, Zhang J C, Yi H M, Zhou X J and Lin C T 2018 *J. Phys.: Condens. Matter.* **30** 125702
- [16] Li M T, Fang Y F, Sun Z, Zhang J C and Lin C T 2018 *J. Phys.: Condens. Matter.* **30** 31LT01
- [17] Nakajima S 1963 *J. Phys. Chem. Solids* **24** 479
- [18] Kriener M, Segawa K, Ren Z, Sasaki S, Wada S, Kuwabata S and Ando Y 2011 *Phys. Rev. B* **84** 054513
- [19] Prozorov R and Kogan V G 2018 *Phys. Rev. Appl.* **10** 014030
- [20] Kirzhner T, Lahoud E, Chaska K B, Salman Z and Kanigel A 2012 *Phys. Rev. B* **86** 064517
- [21] Peng H, De D, Lv B, Wei F and Chu C-W 2013 *Phys. Rev. B* **88** 024515
- [22] Schneeloch J A, Zhong R D, Xu Z J, Gu G D and Tranquada J M 2015 *Phys. Rev. B* **91** 144506
- [23] Vaško A, Tichý L, Horák J and Weissenstein J 1974 *Appl. Phys.* **5** 217
- [24] Koski K J, Cha J J, Reed B W, Wessells C D, Kong D and Cui Y 2012 *J. Am. Chem. Soc.* **134** 7584
- [25] Li Y, Smith N P, Rexhausen W, Schofield M A and Guptasarma P 2019 *J. Phys.: Mater.* **3** 015008
- [26] Zhang H, Liu C-X, Qi X-L, Dai X, Fang Z and Zhang S-C 2009 *Nat. Phys.* **5** 438
- [27] Wan X and Savrasov S Y 2014 *Nat. Commun.* **5** 4144
- [28] Wray L A, Xu S-Y, Xia Y, Hor Y S, Qian D, Fedorov A V, Lin H, Bansil A, Cava R J and Hasan M Z 2010 *Nat. Phys.* **6** 855
- [29] Lahoud E et al 2013 *Phys. Rev. B* **88** 195107
- [30] Tchapkui-Niat J M, Goltzene A and Schwab C 1982 *J. Phys. C: Solid State Phys.* **15** 4671
- [31] Feig M, Nicklas M, Bobnar M, Schnelle W, Schwarz U, Leithe-Jasper A, Hennig C and Gumeniuk R 2018 *Phys. Rev. B* **98** 184516
- [32] Stewart A M 1972 *Phys. Rev. B* **6** 1985
- [33] Goetsch R J, Anand V K, Pandey A and Johnston D C 2012 *Phys. Rev. B* **85** 054517
- [34] Sangeetha N S, Anand V K, Cuervo-Reyes E, Smetana V, Mudring A V and Johnston D C 2018 *Phys. Rev. B* **97** 144403
- [35] Kittel C 2005 *Introduction to Solid State Physics* 8th edn (Hoboken, NJ: Wiley)
- [36] Carlin R L 1986 *Magnetochemistry* ed R L Carlin (Berlin: Springer) p 52
- [37] Chakrabarti D J and Laughlin D E 1981 *Bull. Alloy Phase Diagrams* **2** 305
- [38] Johnston D C 2010 *Adv. Phys.* **59** 803
- [39] Elliot R 1998 *The Physics and Chemistry of Solids* (New York: Wiley) p 603
- [40] Richter W and Becker C R 1977 *Phys. Status Solidi B* **84** 619
- [41] Mulay L N and Boudreaux E A 1976 *Theory and Applications of Molecular Diamagnetism* (New York: Wiley)
- [42] Chalmers B, Christian J W and Massalski T B (ed) 1977 *Metallic Shifts in NMR, Part I* (Progress in Materials Science vol 20) (Oxford: Pergamon) ch 2
- [43] Kriener M, Segawa K, Ren Z, Sasaki S and Ando Y 2011 *Phys. Rev. Lett.* **106** 127004
- [44] Martin C, Craciun V, Miller K H, Uzakbailiy B, Buvaev S, Berger H, Hebard A F and Tanner D B 2013 *Phys. Rev. B* **87** 201201
- [45] Sandilands L J, Reijnders A A, Kriener M, Segawa K, Sasaki S, Ando Y and Burch K S 2014 *Phys. Rev. B* **90** 094503
- [46] Kirshenbaum K, Syers P S, Hope A P, Butch N P, Jeffries J R, Weir S T, Hamlin J J, Maple M B, Vohra Y K and Paglione J 2013 *Phys. Rev. Lett.* **111** 087001
- [47] Bay T V, Naka T, Huang Y K, Luigjes H, Golden M S and de Visser A 2012 *Phys. Rev. Lett.* **108** 057001
- [48] Werthamer N R, Helfand E and Hohenberg P C 1966 *Phys. Rev.* **147** 295
- [49] Yonezawa S, Tajiri K, Nakata S, Nagai Y, Wang Z, Segawa K, Ando Y and Maeno Y 2016 *Nat. Phys.* **13** 123
- [50] Joshi K R, Nusran N M, Tanatar M A, Cho K, Meier W R, Bud'ko S L, Canfield P C and Prozorov R 2019 *Phys. Rev. Appl.* **11** 014035
- [51] Hu C-R 1972 *Phys. Rev. B* **6** 1756
- [52] Liang R, Bonn D A, Hardy W N and Broun D 2005 *Phys. Rev. Lett.* **94** 117001
- [53] Kriener M, Segawa K, Sasaki S and Ando Y 2012 *Phys. Rev. B* **86** 180505
- [54] Matano K, Kriener M, Segawa K, Ando Y and Zheng G-Q 2016 *Nat. Phys.* **12** 852
- [55] Krieger J A, Kanigel A, Ribak A, Pomjakushina E, Chashka K B, Conder K, Morenzoni E, Prokscha T, Suter A and Salman Z 2018 *JPS Conf. Proc.* **21** 011028
- [56] Sundar S, Salem-Sugui S, Chattopadhyay M K, Roy S B, Sharath Chandra L S, Cohen L F and Ghivelder L 2019 *Supercond. Sci. Technol.* **32** 055003
- [57] Barker J A T, Breen B D, Hanson R, Hillier A D, Lees M R, Balakrishnan G, Paul D M and Singh R P 2018 *Phys. Rev. B* **98** 104506
- [58] Carrington A and Manzano F 2003 *Physica C* **385** 205
- [59] Padamsee H, Neighbor J E and Shiffman C A 1973 *J. Low Temp. Phys.* **12** 387
- [60] Johnston D C 2013 *Supercond. Sci. Technol.* **26** 115011
- [61] Wang D M, He J B, Xia T L and Chen G F 2011 *Phys. Rev. B* **83** 132502
- [62] Li M T, Chen L, Feng Z J, Deng D M, Kang B J, Cao S X, Lin C T and Zhang J C 2014 *Physica C* **506** 40
- [63] Fang M-H, Wang H-D, Dong C-H, Li Z-J, Feng C-M, Chen J and Yuan H Q 2011 *Europhys. Lett.* **94** 27009
- [64] Sun L et al 2012 *Nature* **483** 67
- [65] Zhou Y et al 2016 *Phys. Rev. B* **93** 144514
- [66] Orlando T P, McNiff E J, Foner S and Beasley M R 1979 *Phys. Rev. B* **19** 4545
- [67] Meservey R and Schwartz B B 1969 *Superconductivity* ed R D Parks (New York: Marcel Dekker) vol 1 ch 3 p 168
- [68] Kozii V, Bi Z and Ruhman J 2019 *Phys. Rev. X* **9** 031046
- [69] Sohler T, Ponomarev E, Gibertini M, Berger H, Marzari N, Ubrig N and Morpurgo A F 2019 *Phys. Rev. X* **9** 031019
- [70] Gnezdilov V, Pashkevich Y G, Berger H, Pomjakushina E, Conder K and Lemmens P 2011 *Phys. Rev. B* **84** 195118

- [71] Allen P B and Cohen M L 1969 *Phys. Rev.* **177** 704
- [72] Grimaldi C, Pietronero L and Strässler S 1995 *Phys. Rev. Lett.* **75** 1158
- [73] Wang J et al 2019 *Nat. Commun.* **10** 2802
- [74] Mott N F 1990 *Metal Insulator Transitions* (London: Taylor and Francis)
- [75] Kadowaki K and Woods S B 1986 *Solid State Commun.* **58** 507
- [76] Rice M J 1968 *Phys. Rev. Lett.* **20** 1439
- [77] Proust C, Vignolle B, Levallois J, Adachi S and Hussey N E 2016 *Proc. Natl Acad. Sci. USA* **113** 13654
- [78] Hussey N E 2005 *J. Phys. Soc. Japan* **74** 1107
- [79] Maeno Y et al 1997 *J. Phys. Soc. Japan* **66** 1405
- [80] Uemura Y J 1991 *Physica C* **185–189** 733
- [81] Uemura Y J et al 1991 *Phys. Rev. Lett.* **66** 2665
- [82] Hashimoto K et al 2012 *Science* **336** 1554
- [83] Khasanov R, Luetkens H, Amato A, Klauss H-H, Ren Z-A, Yang J, Lu W and Zhao Z-X 2008 *Phys. Rev. B* **78** 092506
- [84] Luetkens H et al 2008 *Phys. Rev. Lett.* **101** 097009
- [85] Drew A J et al 2008 *Phys. Rev. Lett.* **101** 097010
- [86] Pourret A, Malone L, Antunes A B, Yadav C S, Paulose P L, Fauqué B and Behnia K 2011 *Phys. Rev. B* **83** 020504
- [87] Brandt E H 1988 *Phys. Rev. B* **37** 2349
- [88] Petrovic A 2009 Unconventional superconductivity and strong electronic correlations in molybdenum cluster compounds *PhD Thesis* Université de Genève <https://archive-ouverte.unige.ch/unige:14928>
- [89] Barilo S N, Shiryayev S V, Gatalskaya V I, Lynn J W, Baran M, Szymczak R, Szymczak R and Dew-Hughes D 1998 *Phys. Rev. B* **58** 12355
- [90] Huang Z J, Fang H H, Xue Y Y, Hor P H, Chu C W, Norton M L and Tang H Y 1991 *Physica C* **180** 331
- [91] Pambianchi M S, Anlage S M, Hellman E S, Hartford E H, Bruns M and Lee S Y 1994 *Appl. Phys. Lett.* **64** 244
- [92] Uchida T, Nakamura S, Suzuki N, Nagata Y, Mosley W D, Lan M D, Klavins P and Shelton R N 1993 *Physica C* **215** 350
- [93] Hulm J K, Ashkin M, Deis D W and Jones C K 1970 *Progress in Low Temperature Physics* ed C J Gorter (Amsterdam: Elsevier) p 205
- [94] Saghir M, Barker J A T, Balakrishnan G, Hillier A D and Lees M R 2014 *Phys. Rev. B* **90** 064508
- [95] Sosnowski J 1975 *Phys. Status Solidi B* **72** 403
- [96] Dernier P D, Bucher E and Longinotti L D 1975 *J. Solid State Chem.* **15** 203
- [97] Lawson B J, Li G, Yu F, Asaba T, Tinsman C, Gao T, Wang W, Hor Y S and Li L 2014 *Phys. Rev. B* **90** 195141
- [98] Johannes M D and Mazin I I 2008 *Phys. Rev. B* **77** 165135
- [99] Kim H, Min B I and Kim K 2018 *Phys. Rev. B* **98** 144305
- [100] Wagner K E et al 2008 *Phys. Rev. B* **78** 104520
- [101] Zhu X et al 2016 *Sci. Rep.* **6** 26974
- [102] Li S Y, Taillefer L, Hawthorn D G, Tanatar M A, Paglione J, Sutherland M, Hill R W, Wang C H and Chen X H 2004 *Phys. Rev. Lett.* **93** 056401
- [103] Urano C, Nohara M, Kondo S, Sakai F, Takagi H, Shiraki T and Okubo T 2000 *Phys. Rev. Lett.* **85** 1052
- [104] Miyake K, Matsuura T and Varma C M 1989 *Solid State Commun.* **71** 1149
- [105] Nakamae S, Behnia K, Mangkorntong N, Nohara M, Takagi H, Yates S J C and Hussey N E 2003 *Phys. Rev. B* **68** 100502
- [106] Jacko A C, Fjærestad J O and Powell B J 2009 *Nat. Phys.* **5** 422
- [107] Tsujii N, Yoshimura K and Kosuge K 2003 *J. Phys.: Condens. Matter.* **15** 1993
- [108] Tsujii N, Kontani H and Yoshimura K 2005 *Phys. Rev. Lett.* **94** 057201
- [109] Biswas P K et al 2016 *Phys. Rev. B* **93** 220504
- [110] Biswas P K, Guguchia Z, Khasanov R, Chinotti M, Li L, Wang K, Petrovic C and Morenzoni E 2015 *Phys. Rev. B* **92** 195122
- [111] Wang K and Petrovic C 2012 *Phys. Rev. B* **86** 024522
- [112] Sarrao J L and Thompson J D 2007 *J. Phys. Soc. Japan* **76** 051013
- [113] Shang T et al 2019 *Phys. Rev. B* **99** 184513
- [114] Singh D, Barker J A T, Thamizhavel A, Hillier A D, Paul D M and Singh R P 2018 *J. Phys.: Condens. Matter.* **30** 075601
- [115] Mitra S, Okawa K, Kunniniyil Sudheesh S, Sasagawa T, Zhu J-X and Chia E E M 2017 *Phys. Rev. B* **95** 134519
- [116] Biswas P K, Amato A, Baines C, Khasanov R, Luetkens H, Lei H, Petrovic C and Morenzoni E 2013 *Phys. Rev. B* **88** 224515
- [117] Lamura G et al 2013 *Phys. Rev. B* **88** 180509(R)
- [118] Zhang J et al 2016 *Phys. Rev. B* **94** 224502
- [119] Guguchia Z et al 2017 *Nat. Commun.* **8** 1082
- [120] von Rohr F O et al 2019 (arXiv:1903.05292)
- [121] Zaberchik M, Chashka K, Patlgan L, Maniv A, Baines C, King P and Kanigel A 2010 *Phys. Rev. B* **81** 220505
- [122] Wilson M N, Medina T, Munsie T J, Cheung S C, Frandsen B A, Liu L, Yan J, Mandrus D, Uemura Y J and Luke G M 2016 *Phys. Rev. B* **94** 184504
- [123] Uemura Y J et al 2004 (arXiv:0403031)
- [124] Biswas P K, Amato A, Khasanov R, Luetkens H, Wang K, Petrovic C, Cook R M, Lees M R and Morenzoni E 2014 *Phys. Rev. B* **90** 144505
- [125] Pümpin B et al 1990 *Phys. Rev. B* **42** 8019
- [126] Guguchia Z, Khasanov R, Shengelaya A, Pomjakushina E, Billinge S J L, Amato A, Morenzoni E and Keller H 2016 *Phys. Rev. B* **94** 214511
- [127] Homes C C, Clayman B P, Peng J L and Greene R L 1997 *Phys. Rev. B* **56** 5525
- [128] Nugroho A A, Sutjahja I M, Rusydi A, Tjia M O, Menovsky A A, de Boer F R and Franse J J M 1999 *Phys. Rev. B* **60** 15384
- [129] Shengelaya A, Khasanov R, Eshchenko D G, Di Castro D, Savić I M, Park M S, Kim K H, Lee S-I, Müller K A and Keller H 2005 *Phys. Rev. Lett.* **94** 127001
- [130] Homes C C, Lobo R P S M, Fournier P, Zimmers A and Greene R L 2006 *Phys. Rev. B* **74** 214515
- [131] Luetkens H et al 2009 *Nat. Mater.* **8** 305
- [132] Carlo J P et al 2009 *Phys. Rev. Lett.* **102** 087001
- [133] Pratt F L, Baker P J, Blundell S J, Lancaster T, Lewtas H J, Adamson P, Pitcher M J, Parker D R and Clarke S J 2009 *Phys. Rev. B* **79** 052508
- [134] Takeshita S and Kadono R 2009 *New J. Phys.* **11** 035006

- [135] Sheradini Z *et al* 2010 *Phys. Rev. B* **82** 144527
- [136] Guguchia Z, Sheradini Z, Amato A, Maisuradze A, Shengelaya A, Bukowski Z, Luetkens H, Khasanov R, Karpinski J and Keller H 2011 *Phys. Rev. B* **84** 094513
- [137] Wang C N *et al* 2012 *Phys. Rev. B* **85** 214503
- [138] Bendele M *et al* 2010 *Phys. Rev. B* **81** 224520
- [139] Khasanov R *et al* 2008 *Phys. Rev. B* **78** 220510
- [140] Khasanov R, Bendele M, Amato A, Conder K, Keller H, Klaus H H, Luetkens H and Pomjakushina E 2010 *Phys. Rev. Lett.* **104** 087004
- [141] Abdel-Hafiez M, Ge J, Vasiliev A N, Chareev D A, Van de Vondel J, Moshchalkov V V and Silhanek A V 2013 *Phys. Rev. B* **88** 174512
- [142] Kim H *et al* 2010 *Phys. Rev. B* **81** 180503
- [143] Shang T *et al* 2018 *Phys. Rev. Lett.* **121** 257002
- [144] Singh R P, Hillier A D, Mazidian B, Quintanilla J, Annett J F, Paul D M, Balakrishnan G and Lees M R 2014 *Phys. Rev. Lett.* **112** 107002
- [145] Amon A *et al* 2018 *Phys. Rev. B* **97** 014501
- [146] Gross F, Andres K and Chandrasekhar B S 1989 *Physica C* **162–4** 419
- [147] Shu L, MacLaughlin D E, Varma C M, Bernal O O, Ho P C, Fukuda R H, Shen X P and Maple M B 2014 *Phys. Rev. Lett.* **113** 166401
- [148] Ding Z F *et al* 2019 *Phys. Rev. B* **99** 035136